NASA TECHNICAL NOTE

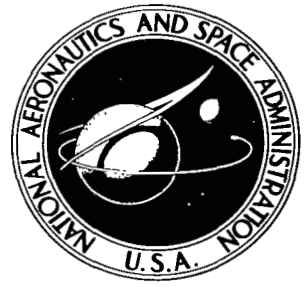

NASA TN D-2123

NASA TN D-2123

ANALYSIS OF MIXING OF COAXIAL STREAMS OF DISSIMILAR FLUIDS INCLUDING ENERGY-GENERATION TERMS

by Herbert Weinstein and Carroll A. Todd

Lewis Research Center
Cleveland, Ohio

NATIONAL AERONAUTICS AND SPACE ADMINISTRATION • WASHINGTON, D. C. • MARCH 1964

ANALYSIS OF MIXING OF COAXIAL STREAMS OF DISSIMILAR FLUIDS INCLUDING ENERGY-GENERATION TERMS

By Herbert Weinstein and Carroll A. Todd

Lewis Research Center
Cleveland, Ohio

NATIONAL AERONAUTICS AND SPACE ADMINISTRATION

For sale by the Office of Technical Services, Department of Commerce,
Washington, D.C. 20230 -- Price $1.50

ANALYSIS OF MIXING OF COAXIAL STREAMS OF DISSIMILAR FLUIDS INCLUDING ENERGY-GENERATION TERMS

By Herbert Weinstein and Carroll A. Todd

SUMMARY

A solution to the problem of the mixing of coaxial flows of dissimilar fluids is presented. The solution is numerical in nature and permits large variations of density, velocity, and temperature of the fluids. It is valid close to or away from the flow inlet.

The system considered is that of a heavy inner fluid surrounded by a light outer stream that is infinite in extent. The fluids may have any initial temperature and velocity profiles, and the flow may be laminar or turbulent in nature. Provision is made for energy generation throughout the flow field. A term is included to permit only axial expansion of the heat-generating fluid to approximate the effect of a cylindrical wall at a relatively large radius.

Results are calculated for various cases to compare the analysis with two sets of experimental data, to illustrate the effect of an approximation of the case with a boundary on the outer stream, and to show the effect of initial input value on the bulk acceleration of the inner-stream fluid. The following results were obtained: The calculated results agreed well with two sets of published data. A different value of the turbulence relation was found for each data set. The boundary wall assumption gave relatively straight streamlines far from the mixing region for cases with heat generation. The containment factor generally increased with increasing molecular-weight ratio and decreased for increasing initial velocity ratio. Internal heat generation decreased containment of the inner-stream fluid.

INTRODUCTION

A solution to the problem of the mixing of coaxial flows of dissimilar fluids is presented in this report. This work has been engendered by the recent interest in the investigation of the coaxial-flow gaseous reactor (ref. 1) and cooled plasma jets (ref. 2). The solution is numerical in nature and permits large initial variations of density, velocity, and temperature of the fluids, and it is valid close to the flow inlet as well as far downstream.

There is a great deal of literature on work on coaxial flows of fluids. This previous work, however, is usually limited in at least one of several ways that prevents its use for the aforementioned problems. The most common

limitation of the previous work is the profile similarity assumption (ref. 3). This assumption limits validity to the region past the potential core. In some of the analyses transformations are made to obtain closed-form solutions that severely limit the variation in flow variables. In reference 4 a closed-form solution for this problem is obtained, but the linearization of transformed equations that is employed again limits the variation in flow variables. The numerical approach is taken in this analysis to avoid these limitations.

The system considered here and shown in figure 1 is that of a heavy inner fluid of circular cross section surrounded by a light outer stream infinite in extent. The fluids may have any initial temperature and velocity profiles, and flow may be laminar or turbulent in nature. Provision is made for energy generation throughout the flow field as a prescribed function of geometric location and concentration of the inner-stream fluid. A term is included in the momentum equation to force an axial expansion of the heat-generating fluid to approximate the effect of a cylindrical wall at a relatively large radius. The transport properties of the fluids are considered to be independent of temperature but are permitted to vary with the concentration of the fluid. No consideration has been given to the hydrodynamic stability of the system or to the aerodynamic compressibility effects.

The analytical portion of this work follows closely the methods established previously by the authors in reference 5. The modifications of the analysis are primarily the inclusion of the energy equation and the effect of temperature variation, along with an extension to include turbulent flow by the introduction of turbulent transport properties (ref. 6). The numerical techniques employed in this report, however, are different from those in reference 5 and are significantly superior. These new techniques provide for greater accuracy and stability in the solution.

The results of this investigation are expressed in terms of a parameter defined in reference 5 called the containment factor. This is the ratio of the amount of inner-stream fluid contained between two planes transverse to the axis compared to the amount that would have been present if there had been no acceleration of the inner stream. This parameter is investigated in regard to its response to varying initial conditions such as velocity ratio, molecular-weight ratio, and energy-generation rate.

The direction taken in the development of this analysis has been, in part, dictated by the lack of experimental data for coaxial flows of fluids with different densities and initial temperatures. Reference 5 is concerned with the isothermal, laminar coaxial flow of fluids of different densities and constitutes the first stage of this analysis. This work was extended to turbulent flow, and both a laminar and a turbulent case were compared with experimental data from the isothermal air-bromine system of reference 6. In the present report, the results of references 5 and 6 are summarized, the analysis is extended to the general case of coaxial flow with prescribed internal heat generation, and the numerical results for the case of coaxial flow of hot and cold airstreams are checked against the experimental results of reference 7. In this manner, the system of momentum and diffusion equations and the system of momentum and energy equations are checked separately. This approach was chosen because no experimental data could be found for the coaxial-flow system with fluids of both different

molecular weights and temperatures. It is felt that good agreement of the analysis with the two special cases would imply the validity of the general solution within the limits set by the assumptions made for the physical properties of the fluids.

SYMBOLS

A,B,C	finite-difference-equation coefficients
$\mathscr{A},\mathscr{B},\mathscr{C},\mathscr{D}$	matrix coefficients
a	wall-assumption constant, equal to either 1 or 0
b_i	constants, i = 1 to 4
c	concentration (mole fraction) of inner-stream component, $c(\psi,z)$
c_p	specific heat, $c_p(\psi,z)$, $c + (1 - c)\overline{c_{p,2}}$
$\overline{c_p}$	initial c_p ratio
D	molecular diffusivity, $D(\psi,z)$
$\overline{F}_1,\overline{F}_2$	inner and outer flow factor to simulate turbulent flow
FF	flow factor for turbulence
G	energy-generation term, $G(\beta,c_p,r,z,u,T,c)$
H	function in energy-generation term
h	enthalpy
$\overline{I}$	containment factor, see eq. (45)
k	thermal conductivity
$\overline{k}_2$	initial conductivity ratio
L	length
m	molecular weight, a constant
$\mathbb{N}/T$	molar density of fluid
n	number of points
Pr	Prandtl number, $c_p\mu/k$
Re	Reynolds number, $\rho\mu r/\mu$
r	radial length variable, $r(\psi,z)$

r_m thickness of mixing region

r_0 initial radius of inner stream

Sc Schmidt number

T temperature, $T(\psi,z)$

$\overline{T}_2$ initial temperature ratio

u axial velocity component, $u(\psi,z)$

V molecular volume

$\overline{V}_2$ molecular volume ratio

v radial velocity component

w mass fraction

x dummy variable

z axial length variable

α prescribed tolerance

β $(m_1/m_2) - 1$

$\gamma_1(r)$ initial velocity distribution

$\gamma_2(r)$ initial concentration distribution

$\gamma_3(r)$ initial temperature distribution

ϵ eddy diffusivity

κ constant in turbulence relation

μ viscosity, $\mu(\psi,z)$

$\overline{\mu}_2$ initial viscosity ratio

ρ mass density

ψ stream function

Subscripts:

i,j points on mesh

max maximum

min minimum

ref reference

t turbulent property

0 initial conditions ($z = 0$)

1 inner stream

2 outer stream

11 self diffusion

12 binary diffusion

Superscripts:

$\bar{}$ normalized to initial inner-stream value, see eq. (7)

$\tilde{}$ transformed energy term

$*$ dummy variable

ANALYSIS

The derivation of the equation set that describes the coaxial-flow system is presented in this section. The numerical methods employed in the solution of these equations are described in the appendix.

Assumptions and Restrictions

The assumptions and restrictions made in deriving the equation set are given by the following list, but not necessarily in order of importance:

(1) The entire flow field is at a constant pressure, and the static and total temperatures are considered equal.

(2) There is axial symmetry in the flow system.

(3) The following molecular fluid properties are independent of temperature: thermal conductivity, viscosity, diffusivity, and heat capacity.

(4) Thermal diffusion is neglected.

(5) The fluids mix ideally; there is no pressure, temperature, or volume change on mixing.

(6) There is a steady state in the system.

(7) The eddy diffusivities of heat, mass, and momentum are equal.

(8) The normal boundary-layer assumptions are used; that is, $\partial u/\partial r \gg \partial u/\partial z$, $u \gg v$, $\partial c/\partial r \gg \partial c/\partial z$, $\partial T/\partial r \gg \partial T/\partial z$, etc.

(9) The assumption $\partial\psi/\partial r \gg \partial\psi/\partial z$, which follows from $u \gg v$, is stated separately because it is used again in a transformation of coordinates.

Other assumptions are made, mainly in the evaluation of physical properties, to obtain a solution from the equation set. These are discussed individually as they are used.

Derivation of Laminar-Flow Equation Set

The following continuity, momentum, diffusion, and energy equations are given for the system shown in figure 1:

Continuity:

$$\frac{\partial}{\partial r}(\rho v r) + \frac{\partial}{\partial z}(\rho u r) = 0 \tag{1}$$

Momentum:

$$v\frac{\partial u}{\partial r} + u\frac{\partial u}{\partial z} = \frac{1}{\rho r}\frac{\partial}{\partial r}\left(r\mu\frac{\partial u}{\partial r}\right) \tag{2}$$

Diffusion:

$$v\frac{\partial w}{\partial r} + u\frac{\partial w}{\partial z} = \frac{1}{\rho r}\frac{\partial}{\partial r}\left(r\rho D_{1,2}\frac{\partial w}{\partial r}\right) \tag{3}$$

Energy:

$$v\frac{\partial h}{\partial r} + u\frac{\partial h}{\partial z} = \frac{1}{\rho r}\frac{\partial}{\partial r}\left(rk\frac{\partial T}{\partial r}\right) + G \tag{4}$$

Each equation is written for variable density and applies over the whole flow field because the gases form a continuum.

The continuity equation already contains the steady-state and axisymmetric assumptions. The momentum equation is the result of simplifying the Navier-Stokes equation with the steady-state, constant-pressure, axisymmetric, and boundary-layer assumptions. The diffusion equation (ref. 8), which contains the steady-state and axisymmetric assumptions but no assumptions as to the variation in density, is correct for large density variations. No pressure diffusion is considered here, as can be noted from equation (1). The energy equation contains the axisymmetric and steady-state assumptions and includes a heat-generation term that is, as yet, unspecified.

Since the fluids mix ideally, the density at a point is equal to the sum of the partial densities at that point. The pressure is constant, and the mass density can be expressed as the molar density multiplied by the molecular weight, $\rho = mN/T$, or, with $m = m_1 c + m_2(1 - c)$, as

$$\rho = \frac{m_2 N}{T}\left[\left(\frac{m_1}{m_2} - 1\right)c + 1\right] \tag{5a}$$

With the substitution $\beta = (m_1/m_2) - 1$, equation (5a) becomes

$$\rho = m_2 N \frac{\beta c + 1}{T} \tag{5b}$$

The mass fraction w is related to the mole fraction c with

$$w = \frac{m_1}{m_2}\frac{c}{\beta c + 1} \tag{6a}$$

and

$$\frac{\partial w}{\partial x} = \frac{m_1}{m_2}\frac{\partial c/\partial x}{(\beta c + 1)^2} \tag{6b}$$

Introducing the dimensionless quantities

$$\left.\begin{array}{lll}
\overline{r} = \dfrac{r}{r_0} & \overline{\mu} = \dfrac{\mu}{\mu_{1,0}} & Sc_{1,0} = \dfrac{\mu_{1,0}}{\rho_{1,0} D_{1,1}} \\[2ex]
\overline{z} = \dfrac{z}{r_0} & \overline{D} = \dfrac{D_{1,2}}{D_{1,1}} & Pr_{1,0} = \dfrac{\mu_1 c_{p,1}}{k_1} \\[2ex]
\overline{u} = \dfrac{u}{u_{1,0}} & \overline{k} = \dfrac{k}{k_{1,0}} & \overline{h} = \dfrac{h}{T_{1,0} c_{p,1,0}} \\[2ex]
\overline{T} = \dfrac{T}{T_{1,0}} & Re_{1,0} = \dfrac{r_0 u_{1,0} \rho_{1,0}}{\mu_{1,0}} & \overline{c_p} = \dfrac{c_p}{c_{p,1,0}} \\[2ex]
\overline{v} = \dfrac{v}{u_{1,0}} & &
\end{array}\right\} \tag{7}$$

and substituting them and equations (5b) and (6b) into equations (1) to (4) yield the following dimensionless equations:

Continuity:

$$\frac{\partial}{\partial r}\left(\overline{rv}\,\frac{\beta c + 1}{\overline{T}}\right) + \frac{\partial}{\partial z}\left(\overline{ru}\,\frac{\beta c + 1}{\overline{T}}\right) = 0 \tag{8}$$

Momentum:

$$\overline{v}\,\frac{\partial \overline{u}}{\partial \overline{r}} + \overline{u}\,\frac{\partial \overline{u}}{\partial \overline{z}} = \frac{1}{Re_{1,0}}\,\frac{\beta + 1}{\beta c + 1}\,\frac{\overline{T}}{\overline{r}}\,\frac{\partial}{\partial \overline{r}}\left(\overline{\mu r}\,\frac{\partial \overline{u}}{\partial \overline{r}}\right) \tag{9}$$

Diffusion:

$$\overline{v}\,\frac{\partial c}{\partial \overline{r}} + \overline{u}\,\frac{\partial c}{\partial \overline{z}} = \frac{\overline{T}(\beta c + 1)}{Re_{1,0}Sc_{1,0}}\,\frac{1}{\overline{r}}\,\frac{\partial}{\partial \overline{r}}\left[\frac{\overline{rD}}{\overline{T}(\beta c + 1)}\,\frac{\partial c}{\partial \overline{r}}\right] \tag{10}$$

Energy:

$$\overline{v}\,\frac{\partial \overline{h}}{\partial \overline{r}} + \overline{u}\,\frac{\partial \overline{h}}{\partial \overline{z}} = \frac{\beta + 1}{Re_{1,0}Pr_{1,0}}\,\frac{\overline{T}}{\beta c + 1}\,\frac{1}{\overline{r}}\,\frac{\partial}{\partial \overline{r}}\left(\overline{kr}\,\frac{\partial \overline{T}}{\partial \overline{r}}\right) + \overline{\overline{G}} \tag{11}$$

where $\overline{\overline{G}}$ is still unspecified. The stream function is defined by

$$\left.\begin{aligned}\frac{\partial \psi}{\partial \overline{z}} &= -\,\overline{rv}\,\frac{\beta c + 1}{\overline{T}} \\ \frac{\partial \psi}{\partial \overline{r}} &= \overline{ru}\,\frac{\beta c + 1}{\overline{T}}\end{aligned}\right\} \tag{12}$$

This satisfies the dimensionless continuity equation.

The momentum, diffusion, continuity, and energy equations are now transformed to the $\overline{z},\psi$-plane with the relations

$$\left.\begin{aligned}\left(\frac{\partial}{\partial \overline{z}}\right)_{\overline{r}} &= \left(\frac{\partial}{\partial z}\right)_{\psi} + \left(\frac{\partial \psi}{\partial z}\right)_{r}\left(\frac{\partial}{\partial \psi}\right)_{\overline{z}} \\ \left(\frac{\partial}{\partial \overline{r}}\right)_{\overline{z}} &= \left(\frac{\partial \psi}{\partial r}\right)_{\overline{z}}\left(\frac{\partial}{\partial \psi}\right)_{\overline{z}}\end{aligned}\right\} \tag{13}$$

Transforming the momentum, diffusion, and energy equations (eqs. (9) to (11)) with equations (12) produces the following equations:

Momentum:

$$\frac{\partial \overline{u}}{\partial \overline{z}} = \frac{\beta + 1}{Re_{1,0}}\,\frac{\partial}{\partial \psi}\left(\overline{\mu r^2 u}\,\frac{\beta c + 1}{\overline{T}}\,\frac{\partial \overline{u}}{\partial \psi}\right) \tag{14}$$

Diffusion:

$$\frac{\partial c}{\partial \bar{z}} = \frac{(\beta c + 1)^2}{Re_{1,0} Sc_{1,0}} \frac{\partial}{\partial \psi} \left(\frac{\bar{r}^2 \overline{Du}}{\bar{T}^2} \frac{\partial c}{\partial \psi} \right) \tag{15}$$

Energy:

$$\frac{\partial h}{\partial z} = \frac{\beta + 1}{Re_{1,0} Pr_{1,0}} \frac{\partial}{\partial \psi} \left(\overline{kr^2 u} \frac{\beta c + 1}{\bar{T}} \frac{\partial \bar{T}}{\partial \psi} \right) + \frac{\overline{TG}}{\bar{u}(\beta c + 1)} \tag{16}$$

Because of the cylindrical geometry, $\bar{r}$ does not drop out of the equations as occurs with Cartesian geometry (ref. 6), and a relation between ψ and $\bar{r}$ must be carried along with the transformed equation set. Since $\partial\psi/\partial\bar{z}$ is zero at $\bar{z} = 0$ and considered very small elsewhere, it is neglected here. From equations (12) is obtained

$$\int_0^{\psi} d\psi^* = \int_0^{\bar{r}} \frac{\bar{u}(\beta c + 1)}{\bar{T}} \bar{r}^* \, dr^* \tag{17}$$

where $*$ denotes the dummy variable. This relation will be used for the initial conditions since they are expressed as functions of $\bar{r}$. For the integration, in which $\bar{r}$ is a dependent variable,

$$\int_0^{r} \bar{r}^* \, dr^* = \int_0^{\psi} \frac{\bar{T}}{\bar{u}(\beta c + 1)} \, d\psi^* \tag{18}$$

is used.

The energy equation is now altered to remove the enthalpy term. Along a streamline

$$\left.\begin{array}{ll} h = h(T,c) & T = T(z) \\ c = c(z) & c_p = c_p(c) \end{array}\right\} \tag{19}$$

The function $c_p(c)$ is taken as

$$c_p(c) = c c_{p,1} + (1 - c) c_{p,2} \tag{20}$$

This is a molar average of a quantity that would normally be taken as a mass average. This approximation provides a linear variation of c_p with c that simplifies the following argument. It is a good approximation when the molecular weights are close together but becomes poor as they diverge. It is also true that

$$h = \int_{T_0}^{T} c_p(c)\,dT^* \tag{21a}$$

and

$$\frac{dh}{dz} = \left(\frac{\partial h}{\partial T}\right)_c \frac{dT}{dz} + \left(\frac{\partial h}{\partial c}\right)_T \frac{dc}{dz} \tag{21b}$$

but

$$\left(\frac{\partial h}{\partial T}\right)_c = c_p(c) \tag{22a}$$

and

$$\left(\frac{\partial h}{\partial c}\right)_T = \int_{T_0}^{T} \left[\frac{\partial c_p(c)}{\partial c}\right]_T dT^* \tag{22b}$$

It is seen from equations (18) that

$$\left.\begin{aligned} \frac{\partial c_p}{\partial c} &= c_{p,1} - c_{p,2} = \text{constant} \\ \left(\frac{\partial h}{\partial c}\right)_T &= (c_{p,1} - c_{p,2}) \int_{T_{ref}}^{T} dT^* = \Delta T(c_{p,1} - c_{p,2}) \end{aligned}\right\} \tag{23}$$

Combining equations (21) to (23) and introducing the dimensionless groups in equation (7) yield

$$\left(\frac{\partial \bar{h}}{\partial \bar{z}}\right)_\psi = \overline{c_p}\left(\frac{\partial \bar{T}}{\partial \bar{z}}\right)_\psi + (1 - \overline{c_{p,2}})\Delta\bar{T}\left(\frac{\partial c}{\partial \bar{z}}\right)_\psi \tag{24}$$

The term $\Delta\bar{T}$ becomes, for a numerical solution, the change in temperature between the mesh points along a streamline.

For the purposes of this report, the generation term is defined as

$$\bar{\bar{G}} = \bar{u}\,\frac{(\beta c + 1)\overline{c_p}}{\bar{T}}\left(b_1 + b_2\,\frac{c}{\bar{T}} + b_3\bar{r}^2 + \frac{b_4}{0.1 + \bar{z}}\right) \tag{25}$$

or

$$\overline{\overline{G}} = \overline{u}\,\frac{\beta c + 1}{\overline{T}}\,\overline{c_p}H$$

where

$$H = b_1 + b_2\,\frac{c}{\overline{T}} + b_3 r^2 + \frac{b_4}{0.1 + \overline{z}}$$

and the b's are input parameters. The b_1 term provides for constant heat generation throughout the flow field and essentially sets the level of heat input. The b_2 term provides for energy generation in just the inner stream, and the coefficient $1/\overline{T}$ corrects for local density variations due to the rising temperature levels. Radial variations of parabolic form are provided for the b_3 term, and the b_4 term provides for an inversely proportional axial dependdence in the heat generation. This form of the generation term allows for both spatial and species variation in the local heat-generation rate. Because of this feature, many different systems can be described or approximated by the equations. Among these are an arc-jet gaining heat energy by recombination (species-dependent generation) and a gaseous reactor with fission occurring in one gas (species-dependent generation) and radiative absorption in the second (outer) gas (approximated by spatially dependent generation).

The energy equation becomes, upon substitution of equations (24) and (25),

$$\overline{c_p}\,\frac{\partial \overline{T}}{\partial \overline{z}} + (1 - \overline{c_{p,2}})\Delta\overline{T}\,\frac{\partial c}{\partial \overline{z}} = \frac{\beta + 1}{Re_{1,0}Pr_{1,0}}\,\frac{\partial}{\partial \psi}\left(\overline{kr^2 u}\,\frac{\beta c + 1}{\overline{T}}\,\frac{\partial \overline{T}}{\partial \psi}\right)$$

$$+ \overline{c_p}\left(b_1 + b_2\,\frac{c}{\overline{T}} + b_3 \overline{r}^2 + \frac{b_4}{0.1 + \overline{z}}\right) \qquad (26)$$

For cases without internal heat generation the streamlines far from the mixing region are unaffected by the mixing process, and the results for the system, which is infinite in the radial direction, apply directly to the case in which both streams are bounded or contained within a cylinder. In the unbounded case with internal heat generation, however, the streamlines bend outward in the radial direction because all the expansion takes place radially. The case of bounded coaxial flow with internal heat generation cannot be approximated with the unbounded case because even far from the mixing region the streamlines are not straight in the unbounded case. For systems in which there is energy generation in either or both of the fluids, it is necessary to modify the equation set so that it can be applied to a system that is finite in the radial direction. To do this rigorously would require the conversion of the problem from an initial-value to a boundary-value problem, but this would greatly complicate the numerical methods involved in the solution. For the coaxial-flow reactor and other systems in which the interesting region of flow is close to the centerline and far from the radial boundary, this boundary can be approximated by a straight streamline at a constant radius. The most important wall condition, that of

zero radial velocity, is satisfied while the conditions of lesser importance, such as zero axial velocity, which are more difficult to satisfy, are ignored. In order to maintain approximately straight streamlines far from the centerline for simulation of channel flow, a term is added to the momentum equation that forces all the gas expansion due to energy generation to occur along a streamline. This addition provides a good description of the expansion process far from the mixing region, where the gradients of velocity and concentration are small, but it is only an approximation in the mixing region, where the gradients are large. In the interest of tractability of the equations, however, the term is defined in the following manner. For continuity along a streamline

$$\rho\bar{u} = \text{constant} \tag{27}$$

Differentiating equation (27) results in

$$\rho\left(\frac{\partial\bar{u}}{\partial\bar{z}}\right)_{\psi} + \bar{u}\left(\frac{\partial\rho}{\partial\bar{z}}\right)_{\psi} = 0$$

The dependence of ρ on concentration can be neglected here, since the energy generation in no way affects concentration. Then

$$\frac{1}{\bar{T}}\frac{\partial\bar{u}}{\partial\bar{z}} = \frac{\bar{u}}{\bar{T}^2}\frac{\partial\bar{T}}{\partial\bar{z}}$$

or

$$\frac{\partial\bar{u}}{\partial\bar{z}} = \frac{\bar{u}}{\bar{T}}\frac{\partial\bar{T}}{\partial\bar{z}} \tag{28}$$

Only the temperature rise due to energy generation is included in this derivation, and the energy equation along the streamline can be written as

$$c_p\frac{\partial\bar{T}}{\partial\bar{z}} = \frac{\overline{TG}}{\bar{u}(\beta c + 1)} \tag{29}$$

Combining equations (28) and (29) yields

$$\frac{\partial\bar{u}}{\partial\bar{z}} = \frac{\bar{G}}{\overline{c_p}(\beta c + 1)} \tag{30}$$

which is the desired term for the axial expansion of the fluid. This term is added to the shear-force term in the momentum equation (14) to yield

$$\frac{\partial\bar{u}}{\partial\bar{z}} = \frac{\beta + 1}{Re_{1,0}}\frac{\partial}{\partial\psi}\left(\overline{\mu r^2 u}\,\frac{\beta c + 1}{\bar{T}}\frac{\partial\bar{u}}{\partial\psi}\right) + \frac{a\bar{G}}{\overline{c_p}(\beta c + 1)} \tag{31}$$

where the factor a in the axial-expansion term is a constant equal to 1 or 0 to allow for the inclusion or the omission of this term. Equation (31) may be

rewritten, with the definition of $\bar{\bar{G}}$, in the form

$$\frac{\partial \bar{u}}{\partial \bar{z}} = \frac{\beta + 1}{Re_{1,0}} \frac{\partial}{\partial \psi} \left(\overline{\mu r^2 u} \frac{\beta c + 1}{\bar{T}} \frac{\partial \bar{u}}{\partial \psi} \right) + \frac{a\bar{u}}{\bar{T}} H \tag{32}$$

Equations (15), (17), (18), (26), and (32) form the set to be integrated from the initial conditions.

The dimensionless transport properties $\bar{D}$, $\bar{\mu}$, and $\bar{k}$ are evaluated from the ratio of the values of the pure components and also, in the cases of viscosity and conductivity, from an elementary mixing equation. This relation is good for low molecular-weight ratios but probably becomes quite poor at higher ratios. This mixing equation is

$$x = \frac{m}{\frac{cm_1}{x_{1,0}} + \frac{(1 - c)m_2}{x_{2,0}}} \tag{33}$$

when expressed in terms of the dummy variable x (ref. 9). For viscosity, the use of equation (33) results in

$$\bar{\mu} = \frac{\beta c + 1}{(\beta + 1)c + \frac{1 - c}{\bar{\mu}_2}} \tag{34}$$

and, for conductivity,

$$\bar{k} = \frac{\beta c + 1}{(\beta + 1)c + \frac{1 - c}{\bar{k}_2}} \tag{35}$$

The dimensionless diffusivity is calculated from the Gilliland equation in the following manner:

$$\bar{D} \equiv \frac{D_{1,2}}{D_{1,1}} = \frac{\left(2V_1^{1/3}\right)^2}{\left(V_1^{1/3} + V_2^{1/3}\right)^2} \sqrt{\frac{m_1}{2}\left(\frac{1}{m_1} + \frac{1}{m_2}\right)}$$

Substituting $\bar{V}_2 = V_2/V_1$ and $m_1/m_2 \approx \beta + 1$ yields

$$\bar{D} = \frac{2\sqrt{2(\beta + 2)}}{\left(1 + \bar{V}_2^{1/3}\right)^2} \tag{36}$$

The dimensionless diffusivity can also be derived from a Lennard-Jones potential argument as shown in reference 5.

The mixing law for the heat capacity of the fluid is expressed by equation (20). It is a simple molar average of the specific heats of the pure components.

Turbulent-Flow Extension

The preceding development for the case of coaxial laminar flow is extended to include the case of turbulent flow by substituting turbulent transport properties for the laminar ones. The turbulent transport properties are defined as

$$\left.\begin{aligned} \mu_t &= \mu\left(1 + \frac{\rho\epsilon}{\mu}\right) \\ D_t &= D\left(1 + \frac{\epsilon}{D}\right) \\ k_t &= k\left(1 + \frac{c_p\rho\epsilon}{k}\right) \end{aligned}\right\} \tag{37}$$

where ϵ is the eddy diffusivity. The eddy diffusivity must be evaluated from a physical argument and experimental data. The particular argument chosen is the accommodation coefficient argument that states (ref. 3, p. 592)

$$\epsilon = \kappa r_m(u_{max} - u_{min}) \tag{38}$$

or that the eddy diffusivity is proportional to the thickness of the mixing region r_m and the velocity decrement across the mixing region. The mixing region thickness can be expressed as a function of the axial position:

$$r_m = r_0 f(\bar{z})$$

For simplicity,

$$f(\bar{z}) = \bar{z}^m$$

(ref. 3, p. 596) and, therefore,

$$r_m = r_0\bar{z}^m \tag{39}$$

Since the region of interest for these calculations is close to the inlet and not much past the potential core, $u_{max} - u_{min}$ is taken to equal the maximum velocity decrement at the initial face:

$$u_{max} - u_{min} = |u_{2,0} - u_{1,0}| \tag{40}$$

Combining equations (37) to (39) yields

$$\epsilon = \kappa r_0 u_{1,0}\bar{z}^m|\bar{u}_2 - 1| \tag{41}$$

It is assumed that the outer stream will affect the turbulence level more than the inner stream. For this reason, the turbulence level for the system is taken as

$$\frac{\rho_{2,0}\epsilon}{\mu_{2,0}} = \frac{\kappa \bar{z}^m r_0 \rho_2 u_{1,0}}{\bar{\mu}_2} \left| \bar{u}_2 - 1 \right|$$

and

$$\frac{r_0 \rho_{2,0} u_{1,0}}{\mu_{2,0}} = \frac{r_0 \rho_{1,0} u_{1,0}}{\mu_{1,0}} \frac{\mu_{1,0}}{\mu_{2,0}} \frac{\rho_{2,0}}{\rho_{1,0}} = \frac{Re_{1,0}}{\bar{\mu}_2(\beta + 1)}$$

or

$$\frac{\rho_{2,0}\epsilon}{\mu_{2,0}} = \kappa \bar{z}^m \frac{Re_{1,0}}{\bar{\mu}(\beta + 1)} \left| \bar{u}_2 - 1 \right| \tag{42}$$

The term $\rho_{2,0}\epsilon/\mu_{2,0}$ is also called the flow factor FF. It is seen that the flow factor is a function of only the initial conditions, the axial position, and the two experimentally determined constants κ and m.

The flow factor is constant with radius at any axial position. The local values of the turbulent transport properties are functions of only the flow-factor variables and the concentration. The dependence on concentration of the turbulent property values is taken to be the same as that used for the laminar values. When equation (27) is used, the local turbulent-transport-property values are

$$\left.\begin{aligned}
\bar{\mu}_t &= \frac{\beta c + 1}{\frac{(\beta + 1)c}{1 + FF} + \frac{1 - c}{(1 + FF)\bar{\mu}_2}} \\
\bar{D}_t &= \frac{\beta c + 1}{\frac{(\beta + 1)c}{\bar{D} + FFSc_{1,0}} + \frac{1 - c}{\bar{D} + FF\bar{\mu}_2 Sc_{1,0}(\beta + 1)}} \\
\bar{k}_t &= \frac{\beta c + 1}{\frac{(\beta + 1)c}{1 + Pr_{1,0}FF} + \frac{1 - c}{\left(1 + \frac{Pr_{1,0}\mu_2 c_{p,2}FF}{\bar{k}_2}\right)\bar{k}_2}}
\end{aligned}\right\} \tag{43}$$

It can be seen by expanding the dimensionless groups that $\rho_{2,0}\epsilon/\mu_2$ can be held constant across a radius, but ϵ becomes a function of the concentration. It is felt that this type of representation is somewhat more correct than that of holding ϵ constant across a radius.

For the cases with energy generation, the temperature level of the system rises, sometimes to a considerable extent. The density of the fluids decreases with increasing axial distance, and the turbulence level of the system is affected. In these cases, the density terms in the mixing equations for the turbulent transport properties are modified to include the $1/T$ variation of density in the following way:

$$\left.\begin{aligned}
\bar{\mu}_t &= \frac{(\beta c + 1)/\bar{T}}{\frac{(\beta + 1)c}{1 + FF} + \frac{1 - c}{(1 + FF)\bar{\mu}_2\bar{T}_2}} \\
\bar{D}_t &= \frac{(\beta c + 1)/\bar{T}}{\frac{(\beta + 1)c}{\bar{D} + FFSc_{1,0}} + \frac{1 - c}{\bar{D} + FFSc_{1,0}\bar{T}_2\bar{\mu}_2(\beta + 1)}} \\
\bar{k}_t &= \frac{(\beta c + 1)/\bar{T}}{\frac{(\beta + 1)c}{1 + FFPr_{1,0}} + \frac{1 - c}{\left(1 + FF\,\frac{Pr_{1,0}\bar{c}_{p,2}\bar{\mu}_2}{\bar{k}_2}\right)\bar{k}_2\bar{T}_2}}
\end{aligned}\right\} \qquad (44)$$

The experimental results obtained from the literature are used to evaluate K, the constant in equation (42), by curve-fitting the data. The value of K is varied until the best fit of the experimental data is obtained. The different values of K for each run are then averaged to obtain a single value of K to use in the calculations.

Some of the results are presented in terms of the containment factor $\bar{I}$

$$\bar{I} = \frac{1}{L}\int_0^L \frac{\left(\int_0^\infty c\bar{r}\,d\bar{r}\right)dz}{\int_0^\infty \bar{u}c\bar{r}\,d\bar{r}} \qquad (45)$$

from reference 3. This parameter is the amount of inner fluid present in a cylindrical section of some very large radius and length L divided by the amount of inner-stream fluid that would have been present in the section had there been no acceleration of the inner stream. This containment factor may vary from a maximum of 1 (no acceleration) to a minimum of $1/\bar{u}_2$.

Program Input

The input to the computer program is the following:

(1) The initial velocity and temperature profiles; when slug flow is

desired, only the velocity and temperature ratios are needed

(2) The molecular-weight ratios of the two streams

(3) The physical properties of the two fluids as ratios, $\overline{u}_2$, $\overline{V}_2$, $\overline{k}_2$, and $c_{p,2}$

(4) The initial values of dimensionless transfer groups, $Re_{1,0}$, $Pr_{1,0}$, and $Sc_{1,0}$

(5) The turbulence-relation constants, m and FF

(6) The constants in the internal heat-generation term, b_i

RESULTS AND DISCUSSION

Accuracy and Limitations

The accuracy of this analysis can be estimated in two ways. First, the size of the various terms discarded in writing the initial equation set may be estimated. When these are small compared to the terms that are kept in the equation set, it is indicated that the assumptions leading to the dropping of these terms are correct. This evaluation was made in reference 3 for the laminar isothermal case, and it gave satisfactorily low values for the derivatives of velocity and temperature in the axial direction compared to the values of these derivatives in the radial direction. This is considered as a validation of the boundary-layer assumptions in the initial equation set for this work, since the momentum and diffusion equations appear in exactly the same form here as they do in reference 3. An exception to this is the axial-expansion term that is sometimes used in the momentum equation. The axial-expansion term is, however, a separate approximation and brings in its own loss of accuracy, which cannot be evaluated here.

The second test of the accuracy of this analysis is whether or not it will fit experimental data. It is important that the predicted values compare with the measured ones, and also that the shapes of predicted curves follow closely those of the experimental curves.

Correlation of Experimental Results

There are relatively few experimental data for the mixing of coaxially flowing fluids that are applicable for a check of this analysis. Two applicable sets of data are selected from the literature for separate specific reasons. Since no published experimental work could be found for the case of simultaneous heat, mass, and momentum transfer, one of the cases chosen is for combined heat and momentum transfer, and the other is for combined mass and momentum transfer. There is also no experimental work for energy-generating gases, so the calculated results for the cases with energy generation stand without any conclusive evidence of an accurate formulation of the problem.

The work of reference 7 for a hot-air - cold-air coaxial-flow system was chosen as representative of combined heat- and momentum-transfer data because of the effort made to obtain initial slug-flow velocity profiles in the equipment and because velocity and temperature profiles were supplied. The air-bromine data of reference 6 were chosen for the combined mass- and momentum-transfer data because of the high molecular-weight ratio (about 5) of the two fluids used.

Figure 2 shows typical data from reference 7 with the curve fit from the analysis. In figure 2(a) the velocity profiles show very good agreement between data and analysis. The trends of the data are fitted very well by the analytical curves with a single value of κ. The corresponding temperature profiles are shown in figure 2(b). The agreement is not as good as in the velocity profiles because of the deviation of the analytical curve from the data at an axial station of $\bar{z} = 13.3$. This deviation would almost vanish, however, if the asymmetry in the data were removed. This is illustrated in the figure 2(b) by the square data points, which are the original data moved inward until the peak-temperature data point fall on the flow axis. For the three applicable cases of reference 7, the value of κ obtained was 0.0047 ± 0.0002 with the exponent $m = 1/2$.

The work of reference 6 is actually a special case of the present analysis. The analysis of reference 6 is smaller in scope, but the equation set derived here reduces to the set derived there. Figure 3(a) shows average concentration against axial distance for a case that appeared to be laminar flow along with the analytical curve calculated with the same initial conditions. The agreement is very good. Figure 3(b) shows data for a turbulent run along with the best-fit analytical curve. The axial variation of $\rho\epsilon/\mu$ is taken independent of z in reference 6, and the calculated value of κ is 0.108. There is very poor agreement between the two sets of data since, even after correcting in an approximate way for the axial variation of $\rho\epsilon/\mu$, there is a factor of 5 between the two values of the constants. This discrepancy cannot be rectified until more data become available for various systems. In the following calculations, the values of the empirical constants obtained from the data of reference 7 will be used because those data include velocity and temperature profiles.

The good agreement between the data and the analysis does not constitute a validation of the physical-property assumptions because the energy-equation check was based on data for a system with a molecular-weight ratio of 1.

Sample Results and Discussion of Heat-Generation Terms

Calculations were made with the computer program to illustrate the effects of the heat-generation terms in the equation set and to present some sample results.

Figures 4 to 10 are concerned with six cases computed from the analysis. They all have the same physical-property input, the same initial velocity and molecular-weight ratios, and the same flat temperature profiles. They differ in that there are laminar and turbulent flows for each of the three cases with varying energy-generation terms. The first case has no internal energy generation; the second has a prescribed generation rate in the inner stream, but does not

include the wall-assumption term; and the third case has the same heat-generation rate as the second case, but also includes the wall-assumption term.

Figure 4 shows velocity profiles for three cases of laminar flow with almost similar initial conditions. Figure 4(a) is a case with no heat generation; figure 4(b) is a case with heat generation, but with $a = 0$ (no wall assumption); and figure 4(c) is a case with the same heat generation and the wall assumption ($a = 1$).

The profiles for all three cases are smooth S-shaped curves after the initial face. The important characteristics of the curves are the acceleration of the central streamline and the momentum spreading of the inner stream. The case with no heat generation shows an undisturbed central streamline and very little spreading of the inner stream at an axial station 27.89 radii downstream ($\bar{z} = 27.89$). For the case of heat generation and $a = 0$, the central streamline is again undisturbed, but the inner stream has spread to more than double its initial radius at $\bar{z} = 26.08$. Since this is essentially free jet flow, all the expansion due to heating takes place radially. The case of heat generation with $a = 1$, however, shows a central streamline accelerated to about six times the initial velocity and a spreading of the inner stream, which is slightly more than for the case of no heat generation, but much less than for the case of $a = 0$.

Three cases of turbulent flow with initial conditions that were identical to the laminar ones, except for the turbulence condition, were also computed. The velocity profiles are shown in figure 5. For the case of no heat generation (fig. 5(a)), the center streamline has been accelerated to about 28 times the initial value at $\bar{z} = 26.52$, and the mixing region extends farther into the inner stream so that the inner stream appears to have shrunk a little in radius. The case of heat generation and $a = 0$ (fig. 5(b)) exhibits a central streamline that has been accelerated to a value about 24 times the initial value and a small amount of spreading of the inner stream at $\bar{z} = 29.77$. The central streamline acceleration in the case of no heat generation is an indication of the magnitude of the momentum diffusivity effect, since there is no temperature-induced acceleration. The central streamline acceleration in the case of heat generation with $a = 0$ is an indication of the magnitude of the effect of the temperature rise, since the inner stream is spreading and the central streamline is not affected much by the outer stream at these relatively low values of $\bar{z}$. This is borne out in figure 5(c), which shows the velocity profiles for the case of heat generation with $a = 1$. The central streamline has accelerated to a velocity about 38 times the initial value, which is considerably more than that in either figure 5(a) or (b). This large value is due to the combined effects of the momentum diffusivity and the temperature rise. The inner stream has shrunk slightly in radius so that the outer stream has had more of a chance to act on the central streamline than in the case with $a = 0$.

The concentration profiles for the cases just discussed are shown in figures 6 and 7 for laminar and turbulent flow, respectively. The important characteristics in these figures are the centerline concentration (mole fraction) and the mass spreading of the inner stream. Figure 6(a) is the case of no heat generation. The centerline concentration is about 0.41 at $\bar{z} = 27.89$, and the inner stream has shrunk slightly in radius. In figure 6(b), the case of heat generation with $a = 0$, the centerline concentration is about 0.59 at $\bar{z} = 26.08$, and

the inner stream has spread to about double its initial radius. In figure 6(c), the case of heat generation with $a = 1$, the centerline concentration is about 0.64 at $\overline{z} = 27.49$, and the inner stream has spread only slightly from its initial radius. It is important to note that the inclusion of the heat-generation term for the laminar cases leads to higher centerline concentrations. This is due to temperature-induced acceleration, which causes the inner-stream fluid to spend less time in the region $0 \leq \overline{z} \leq 30$, and there is less mass transfer in the region.

Figure 7 shows the turbulent-flow cases with centerline velocities of about 0.15 to 0.20 at $\overline{z} \approx 28$ and large inner-stream shrinkage for no heat generation, slight shrinkage for heat generation and $a = 0$, and moderate shrinkage for heat generation and $a = 1$. In turbulent flow, the eddy diffusivity is relatively so large that the interesting effect noted previously is masked.

The temperature profiles for the same cases are shown in figures 8 and 9 for laminar and turbulent flow, respectively. Only the cases with heat generation are shown, since the initial temperature profiles in these cases were flat. Figures 8(a) and (b) are for laminar flow with $a = 0$ and $a = 1$, respectively. The only observation of any importance to be made is the relative spreading of inner-stream temperature. In figure 8(a), the inner stream has spread to almost double its initial radius at $\overline{z} = 26.08$, and the mixing region is thin, as shown by the sharp cutoff in temperature. In figure 8(b), the inner stream has spread only slightly at $\overline{z} = 27.49$, and the mixing region is still relatively thin. For the turbulent-flow cases of figures 9(a) and (b), the spreading is much less pronounced, and the mixing region is quite large, on the order of the inner-stream initial-radius size, at a $\overline{z}$ of about 29. For both cases the inner stream has shrunk to some extent.

The streamlines for the cases just discussed show clearly the value of the wall-assumption term. This is a term added to the momentum equation that, when $a = 1$, forces all the fluid expansion due to energy generation to occur along a streamline.

Figure 10(a) shows streamlines for the three cases of laminar flow. The solid lines (for the case of $a = 0$) depart greatly from the circles representing the case of no heat generation. The dashed lines representing the case of $a = 1$ follow closely the values for no heat generation at values of $\overline{r}$ of about 0.3 and 2. Since the wall assumption is poor in the mixing region and no useful comparison can be made with values there, the case with no heat generation is not shown near an $\overline{r}$ of 1.

For turbulent flow (fig. 10(b)), the case with $a = 1$ again falls closer to the no-heat-generation values than the case with $a = 0$. For turbulent flow, however, the divergence of any one case from any other is small. It should be emphasized that all that is shown in figure 10(b) is that the wall assumption does straighten out the streamlines of cases with heat generation so that they approximate the streamlines that would occur with an actual wall present. No comparison with experimental data is made to show the accuracy of the assumption.

Inner-Stream Containment

Figure 11 shows plots of inner-stream containment as a function of initial-velocity ratio. Figures 11(a) and (b) are for cases of heat generation only in the inner stream and laminar and turbulent flow, respectively. It is seen for both cases that increasing the molecular weight of the inner stream and decreasing the initial velocity ratio increase the containment factor.

For turbulent flow the variation in $\overline{u}_2$ has a greater effect than for laminar flow. Also, the values of the containment factor are only slightly higher for laminar flow than for turbulent flow at low values of $\overline{u}_2$ (less than about 5). When $\overline{u}_2$ is large, however, the laminar values are several times larger than the turbulent ones. For the case of heat generation in both streams and laminar flow, increasing the initial velocity ratio decreases the containment factor, but not to the same extent as for heat generation in the inner stream only. This is due to the fact that the whole system is accelerating in the former case and the fluids spend less time in the region of interest. It is also seen that the molecular-weight variation has no clear effect on the containment factor. The reason is that the pure-component specific-heat ratio varies inversely with molecular weight for ideal gases, and this variation absorbs a great deal of the effect of the molecular-weight variation. The final case of heat generation in both streams with turbulent flow shows characteristics similar to those in the case of heat generation in one stream with turbulent flow. The containment factor decreases with increasing $\overline{u}_2$ and increases with increasing β. The values of the containment factor are lower for this case, however, since both streams are accelerating and the momentum transfer is greater.

SUMMARY OF RESULTS

In this report, an analysis of the mixing of coaxial streams of dissimilar fluids is presented. The analysis is based on certain assumptions such as boundary-layer simplifications, constant pressure in the flow field, a simple approximation for a boundary wall for cases with internal heat generation to simulate channel flow, and a given turbulence relation. The analysis yielded an equation set that was solved numerically. The results were checked against two sets of experimental results, and the wall assumption used was evaluated as to its effect on the flow. The following results were obtained:

1. The calculated values agreed well with two sets of published data.

2. For the data of NASA MEMO 12-21-58E, for coaxial hot and cold airflow, the turbulence relation obtained was

$$\frac{\rho_{2,0}\epsilon}{\mu_{2,0}} = (0.0047 \pm 0.0002)\overline{z}^{1/2} \frac{\mathrm{Re}_{1,0}}{\overline{\mu}_2(\beta + 1)} \left|\overline{u}_2 - 1\right|$$

where $\rho_{2,0}$ is the outer-stream mass density at $z = 0$, ϵ is the eddy diffusivity, $\mu_{2,0}$ is the outer-stream viscosity at $z = 0$, $\overline{z}$ is the dimensionless axial length variable, $\mathrm{Re}_{1,0}$ is the inner-stream Reynolds number at $z = 0$,

$\bar{\mu}_2$ is the dimensionless outer-stream viscosity, β is a molecular-weight factor, and $\bar{u}_2$ is the dimensionless outer-stream axial velocity component. This relation was used for the remaining calculations.

3. The data of Ragsdale and Weinstein for coaxial flow of bromine and air yielded the turbulence relation

$$\frac{\rho_{2,0}\epsilon}{\mu_{2,0}} = 0.108 \frac{Re_{1,0}}{\bar{\mu}_2(\beta + 1)} |\bar{u}_2 - 1|$$

There was poor agreement between the hot-air - cold-air correlation and the bromine-air correlation even after the z dependence was included in the latter.

4. The wall assumption, which consisted of forcing all the expansion caused by energy generation to occur along a streamline, gave relatively straight streamlines far from the mixing region, as was desired.

5. The containment factor generally increased with increasing molecular-weight ratio and decreased with increasing initial velocity ratio.

6. The containment factor decreased with increasing internal heat-generation rate and was affected more by heat generation in the outer stream than by heat generation in the inner stream.

Lewis Research Center
National Aeronautics and Space Administration
Cleveland, Ohio, October 22, 1963

APPENDIX - NUMERICAL METHOD

In the following discussion all bars are deleted as a matter of convenience.

The equations describing the hydrodynamic system are

Momentum:

$$\frac{\partial u}{\partial z} = \frac{\beta + 1}{Re} \frac{\partial}{\partial \psi} \left(r^2 \mu u \frac{\beta c + 1}{T} \frac{\partial u}{\partial \psi} \right) + \frac{aG}{c_p(\beta c + 1)} \tag{A1}$$

Diffusion:

$$\frac{\partial c}{\partial z} = \frac{(\beta c + 1)^2}{ReSc} \frac{\partial}{\partial \psi} \left(\frac{Dr^2 u}{T} \frac{\partial c}{\partial \psi} \right) \tag{A2}$$

Energy:

$$(1 - c_{p,2})\Delta T \frac{\partial c}{\partial z} + c_p \frac{\partial T}{\partial z} = \frac{\beta + 1}{ReSc} \frac{\partial}{\partial \psi} \left(kr^2 u \frac{\beta c + 1}{T} \frac{\partial T}{\partial \psi} \right) + \frac{TG}{u(\beta c + 1)} \tag{A3}$$

Continuity:

$$r^2 = 2 \int_0^{\psi} \frac{T \, d\psi'}{u(\beta c + 1)} \tag{A4}$$

where

$$\mu = \frac{(\beta c + 1)/T}{\dfrac{(\beta + 1)c}{1 + F_1} + \dfrac{1 - c}{\mu_2 T_2 (F_2 + 1)}}$$

$$G = u \frac{\beta c + 1}{T} c_p \left(V_1 + V_2 \frac{c}{T} + V_3 r^2 + \frac{V_4}{1 + z} \right)$$

$$D = \frac{\beta c + 1}{\dfrac{(\beta + 1)c}{D_1 + F_1 Sc} + \dfrac{1 - c}{D_1 + F_2 \mu_2 Sc(\beta + 1)}}$$

$$D_1 = \frac{2 \sqrt{2(\beta + 2)}}{\left(1 + V_2^{1/3} \right)^2}$$

$$a = \begin{cases} 1 & \text{includes heat-generation term in eq. (A1)} \\ 0 & \text{excludes heat-generation term in eq. (A1)} \end{cases}$$

$$k = \frac{(\beta c + 1)/T}{\dfrac{(\beta + 1)c}{1 + PrF_1} + \dfrac{1 - c}{\left(1 + \dfrac{Pr\mu_2 c_{p,2} F_2}{k_2}\right) k_2 T_2}}$$

The solutions of equations (A1) to (A4) are to be found on the finite strip ($0 \le \psi \le \psi_{max}$, $0 \le z \le z_{max}$), given the following boundary and initial conditions:

$$\frac{\partial u}{\partial \psi} = \frac{\partial c}{\partial \psi} = \frac{\partial T}{\partial \psi} \equiv 0 \qquad \text{for} \quad \psi = 0 \tag{A5}$$

$$\left.\begin{aligned} u(\psi_{max}, z) &= u_2 \\ T(\psi_{max}, z) &= T_2 \\ c(\psi_{max}, z) &= 0 \end{aligned}\right\} \tag{A6}$$

where u_2 and T_2 are prescribed velocity and temperature ratios, and

$$\left.\begin{aligned} u(\psi, 0) &= \gamma_1(\psi) \\ c(\psi, 0) &= \gamma_2(\psi) \\ T(\psi, 0) &= \gamma_3(\psi) \end{aligned}\right\} \tag{A7}$$

where γ_1, γ_2, and γ_3 are specified as

$$\gamma_1(r) = \begin{cases} 1 & 0 \le r \le 1 \\ U_2 & 1 \le r \le r_{max} \end{cases} \tag{A8}$$

$$\gamma_2(r) = \begin{cases} 1 & 0 \le r \le 1 \\ 0 & 1 \le r \le r_{max} \end{cases} \tag{A9}$$

$$\gamma_3(r) = \begin{cases} 1 & 0 \le r \le 1 \\ T_2 & 1 < r < r_{max} \end{cases} \tag{A10}$$

Since

$$r^2 = \int_0^{\psi} \frac{2T\, d\psi'}{u(\beta c + 1)}$$

equations (A8) to (A10) can be determined in terms of ψ:

$$r_1(\psi) = \begin{cases} 1 & 0 \le \psi \le \dfrac{\beta + 1}{2} \\ u_2 & \dfrac{\beta + 1}{2} \le \psi \le \psi_{max} \end{cases} \tag{A11}$$

$$r_2(\psi) = \begin{cases} 1 & 0 \le \psi \le \dfrac{\beta + 1}{2} \\ 0 & \dfrac{\beta + 1}{2} \le \psi \le \psi_{max} \end{cases} \tag{A12}$$

$$r_3(\psi) = \begin{cases} 1 & 0 \le \psi \le \dfrac{\beta + 1}{2} \\ T_2 & \dfrac{\beta + 1}{2} \le \psi \le \psi_{max} \end{cases} \tag{A13}$$

Correspondingly, $r(\psi,0)$ can be defined as

$$r(\psi,0) = \begin{cases} \sqrt{\dfrac{2\psi}{\beta + 1}} & 0 \le \psi \le \dfrac{\beta + 1}{2} \\ \sqrt{1 + \dfrac{2T_2}{u_2}\left(\psi - \dfrac{\beta + 1}{2}\right)} & \dfrac{\beta + 1}{2} \le \psi \le \psi_{max} \end{cases} \tag{A14}$$

With c^*, U^*, T^*, and r^* defined as approximate solution vectors of equations (A1) to (A4) at some length z, equation (A1) can be rewritten in a linearized form as

$$\frac{\partial u}{\partial z} = \frac{\beta + 1}{Re} \frac{\partial}{\partial \psi}\left(r^{*2}\mu^* u^* \frac{\beta c^* + 1}{T^*} \frac{\partial u}{\partial \psi}\right) + \frac{aG^*}{c_p^*(\beta c^* + 1)} \tag{A15}$$

or

$$\frac{\partial u}{\partial z} = A_u(\psi) \frac{\partial}{\partial \psi}\left(B_u(\psi) \frac{\partial u}{\partial \psi}\right) + C_u(\psi) \tag{A16}$$

where

$$\left.\begin{aligned} A_u(\psi) &= \frac{\beta + 1}{Re} \\ B_u(\psi) &= r^{*2}\mu^* u^* \frac{\beta c^* + 1}{T^*} \\ C_u(\psi) &= \frac{aG^*}{c_p^*(\beta c^* + 1)} \end{aligned}\right\} \tag{A17}$$

Similarly, equations (A2) and (A3) can be put into the form of equation (A16) with coefficients defined as

$$\left.\begin{aligned} A_c(\psi) &= \frac{(\beta c^* + 1)^2}{Re} \\ B_c(\psi) &= \frac{D^* r^{*2} u^*}{T} \\ C_c(\psi) &= 0 \end{aligned}\right\} \tag{A18}$$

and

$$\left.\begin{aligned} A_T(\psi) &= \frac{\beta + 1}{RePr\left[(1 - c_{p,2})\Delta z \frac{\partial c^*}{\partial z} + c_p^*\right]} \\ B_T(\psi) &= \frac{k^* r^{*2} u^* (\beta c^* + 1)}{T^*} \\ C_T(\psi) &= \frac{T^* G^*}{u^*(\beta c^* + 1)\left[(1 - c_{p,2})\Delta z \frac{\partial c^*}{\partial z} + c_p^*\right]} \end{aligned}\right\} \tag{A19}$$

With the strip R overlayed with a number of rectangles of dimensions $\Delta\psi$ by Δz, a grid or mesh is constructed. If the notation $R_{i,j}$ denotes the i^{th}, j^{th} point on the mesh, then $u(\psi_i, z_j) \equiv u_{i,j}$ can be defined as the functional value of $u(\psi,z)$ associated with the grid point $R_{i,j}$.

Using equation (A16) as a general form and expanding give

$$\frac{\partial u}{\partial z} = A\left(B \frac{\partial^2 u}{\partial \psi^2} + \frac{dB}{d\psi} \frac{\partial u}{\partial \psi}\right) + C \tag{A20}$$

The derivative approximates at a point $R_{i,j}$ are defined implicitly as

$$\left(\frac{\partial u}{\partial z}\right)_{i,j+1} = \frac{u_{i,j+1} - u_{i,j}}{\Delta z} \tag{A21}$$

$$\left(\frac{\partial u}{\partial \psi}\right)_{i,j+1} = \frac{u_{i+1,j+1} - u_{i-1,j-1}}{2\,\Delta\psi} \tag{A22}$$

$$\left(\frac{\partial^2 u}{\partial \psi^2}\right)_{i,j+1} = \frac{u_{i+1,j+1} - 2u_{i,j+1} + u_{i-1,j+1}}{\Delta\psi^2} \tag{A23}$$

Substitution of equations (A21) to (A23) into equation (A20) yields

$$\left[\frac{A_i B_i}{\Delta\psi^2} - \frac{(B_{i+1} - B_{i-1})}{4\,\Delta\psi^2}\right] u_{i-1,j+1} - \left(\frac{2A_i B_i}{\Delta\psi^2} + \frac{1}{\Delta z}\right) u_{i,j+1} + \left(\frac{A_i B_i}{\Delta\psi^2} + \frac{B_{i+1} - B_{i-1}}{4\,\Delta\psi^2}\right) u_{i+1,j+1} = -c_i - \frac{u_{i,j}}{\Delta z} \tag{A24}$$

Equation (A24) is valid only on the interior of the grid (i.e., $i = 2,3, \ldots, n-1$). The boundary conditions (e.g., eqs. (A5) and (A6)) must be applied to obtain similar equations at $i = 1$ and n. Hence, applying equation (A5) to equation (A20) results in

$$-\left(\frac{B_1}{\Delta\psi^2} - \frac{1}{\Delta z}\right) u_{1,j+1} + \frac{B_1}{\Delta\psi^2} u_{2,j+1} = -c_1 - \frac{u_{1,j}}{\Delta z} \tag{A25}$$

and utilizing equation (A6) yields

$$\left(\frac{A_n B_n}{\Delta\psi^2} - \frac{\omega - B_{i-1}}{4\,\Delta\psi^2}\right) u_{n-1,j+1} - \left(\frac{2A_n B_n}{\Delta\psi^2} + \frac{1}{\Delta z}\right) u_{n,j+1} = -\left(\frac{A_n B_n}{\Delta\psi^2} + \frac{\omega - B_{n-1}}{4\,\Delta\psi^2}\right) u_2 - c_n - \frac{u_{n,j}}{\Delta z} \tag{A26}$$

where ω is $B_u(\psi_{max})$ as given by equation (A17).

When i varies from 1 to n (i.e., $\psi = 0$ to $\psi = \psi_{max}$), a linear tridiagonal system of equations is generated of the form

$$\begin{bmatrix} \mathscr{B}_1 & \mathscr{C}_1 & 0 & \cdots & & 0 \\ \mathscr{A}_2 & \mathscr{B}_2 & \mathscr{C}_2 & 0 & \cdots & 0 \\ 0 & \mathscr{A}_3 & \mathscr{B}_3 & \mathscr{C}_3 & 0 & \cdots & 0 \\ & & \ddots & \ddots & \ddots & & \\ & & & \ddots & \ddots & \ddots & \\ & & & & \ddots & \ddots & \mathscr{C}_{n-1} \\ 0 & & & & & \mathscr{A}_n & \mathscr{B}_n \end{bmatrix} \begin{bmatrix} u_{1,j+1} \\ u_{2,j+1} \\ u_{3,j+1} \\ \vdots \\ u_{n,j+1} \end{bmatrix} = \begin{bmatrix} \mathscr{D}_1 \\ \mathscr{D}_2 \\ \mathscr{D}_3 \\ \vdots \\ \mathscr{D}_n \end{bmatrix} \tag{A27}$$

with

$$\left.\begin{aligned} \mathscr{A}_i &= \frac{A_i B_i}{\Delta\psi^2} - \frac{B_{i+1} - B_{i-1}}{4\,\Delta\psi^2} \qquad i = 2,3, \ldots, n-1 \\ \mathscr{A}_n &= \frac{A_n B_n}{\Delta\psi^2} - \frac{\omega - B_{n-1}}{4\,\Delta\psi^2} \end{aligned}\right\} \tag{A28}$$

$$\left.\begin{aligned} \mathscr{B}_1 &= \frac{B_1}{\Delta\psi^2} \\ \mathscr{B}_i &= -\frac{2A_i B_i}{\Delta\psi^2} + \frac{1}{\Delta z} \qquad i = 2,3, \ldots, n \end{aligned}\right\} \tag{A29}$$

$$\left.\begin{aligned} \mathscr{C}_1 &= \frac{B_1}{\Delta\psi^2} \\ \mathscr{C}_i &= \frac{A_i B_i}{\Delta\psi^2} + \frac{B_{i+1} - B_{i-1}}{4\,\Delta\psi^2} \qquad i = 2,3, \ldots, n-1 \end{aligned}\right\} \tag{A30}$$

$$\left.\begin{aligned} \mathscr{D}_i &= -\mathscr{C}_i - \frac{u_{i,j}}{\Delta z} \qquad i = 1,2, \ldots, n-1 \\ \mathscr{D}_n &= -\left(\frac{A_n B_n}{\Delta\psi^2} + \frac{\omega - B_{n-1}}{4\,\Delta\psi^2}\right) u_2 - C_n - \frac{u_{n,j}}{\Delta z} \end{aligned}\right\} \tag{A31}$$

The solution of equation (A27) is effected by triangularizing the matrix and by a back substitution. Triangularization is accomplished by the transformation

$$\left.\begin{aligned} \mathscr{B}_1' &= \mathscr{B}_1 \\ \mathscr{B}_i' &= \mathscr{B}_i - \frac{\mathscr{A}_i \mathscr{C}_{i-1}}{\mathscr{B}_{i-1}'} \qquad i = 2,3, \ldots, n \\ \mathscr{D}_1' &= \mathscr{D}_1 \\ \mathscr{D}_i' &= \mathscr{D}_i - \frac{\mathscr{A}_i \mathscr{D}_{i-1}}{\mathscr{B}_{i-1}'} \qquad i = 2,3, \ldots, n \end{aligned}\right\} \tag{A32}$$

The back substitution is effected by

$$\left.\begin{aligned} u_{n,j+1} &= \frac{\mathscr{D}_n'}{\mathscr{B}_n'} \\ u_{i,j+1} &= \frac{\mathscr{D}_i' - \mathscr{C}_i u_{i+1,j+1}}{\mathscr{B}_i'} \qquad i = n-1, n-2, \ldots, 1 \end{aligned}\right\} \tag{A33}$$

If a similar argument is followed, solution vectors of $C_{i,j+1}$ and $T_{i,j+1}$ can be computed. Define

$$\left.\begin{aligned} \Delta_1 &= |u^*_{i,j+1} - u_{i,j+1}| \\ \Delta_2 &= |C^*_{i,j+1} - C_{i,j+1}| \\ \Delta_3 &= |T^*_{i,j+1} - T_{i,j+1}| \end{aligned}\right\} \tag{A34}$$

If Δ_1, Δ_2, and $\Delta_3 < \alpha$, where α is some prescribed tolerance, the solution to equations (A1) to (A4) have been effected for a given z. If $\Delta_i > \alpha$, however, the coefficients A, B, and C of equations (A17) to (A19) may be computed with the values of $u_{i,j+1}$, $C_{i,j+1}$, and $T_{i,j+1}$. The iteration procedure is then repeated until convergence is obtained.

The iteration procedure was programmed in Fortran II for the IBM 7090. Although the stability of the solution is guaranteed by the use of the implicit scheme, truncation error is governed by the size of Δz. It was found that the iteration procedure converged to a tolerance α of 10^{-4} within three or four trials. The time of running a particular solution is, of course, determined by the case input parameters; generally, however, the time required to complete a solution to an axial length of 30 is about 1.5 to 2 minutes.

REFERENCES

1. Weinstein, Herbert, and Ragsdale, Robert G.: A Coaxial Flow Reactor - A Gaseous Nuclear-Rocket Concept. Preprint 1518-60, Am. Rocket Soc., Inc., 1960.

2. Grey, Jerry: Heat Transfer from an Ionized Gas to a Gaseous Coolant. Rep. 437-A, Aero. Eng. Lab., Princeton Univ., July 1959.

3. Schlichting, H.: Boundary Layer Theory. McGraw-Hill Book Co., Inc., 1960.

4. Kleinstein, Gdalia: An Approximate Solution for the Axisymmetric Jet of a Laminar Compressible Fluid. Quarterly Appl. Math., vol. 20, no. 1, Apr. 1962, pp. 49-54.

5. Weinstein, Herbert, and Todd, Carroll A.: A Numerical Solution of the Problem of Mixing of Laminar Coaxial Streams of Greatly Different Densities - Isothermal Case. NASA TN D-1534, 1963.

6. Ragsdale, Robert G., and Weinstein, Herbert: On the Hydrodynamics of a Coaxial Flow Gaseous Reactor. Proc. ARS/ANS/IAS Nuclear Prop. Conf., Aug. 1962, TID 7653, pt. 1, pp. 82-88.

7. Burley, Richard R., and Bryant, Lively: Experimental Investigation of Coaxial Jet Mixing of Two Subsonic Streams at Various Temperature, Mach Number, and Diameter Ratios for Three Configurations. NASA MEMO 12-21-58E, 1959.

8. Bird, R. Byron, Steward, Warren E., and Lightfoot, Edwin C.: Notes on Transport Phenomena. John Wiley & Sons, Inc., 1958.

9. Hirschfelder, Joseph O., Curtiss, Charles F., and Bird, R. Byron: Molecular Theory of Gases and Liquids. John Wiley & Sons, Inc., 1954.

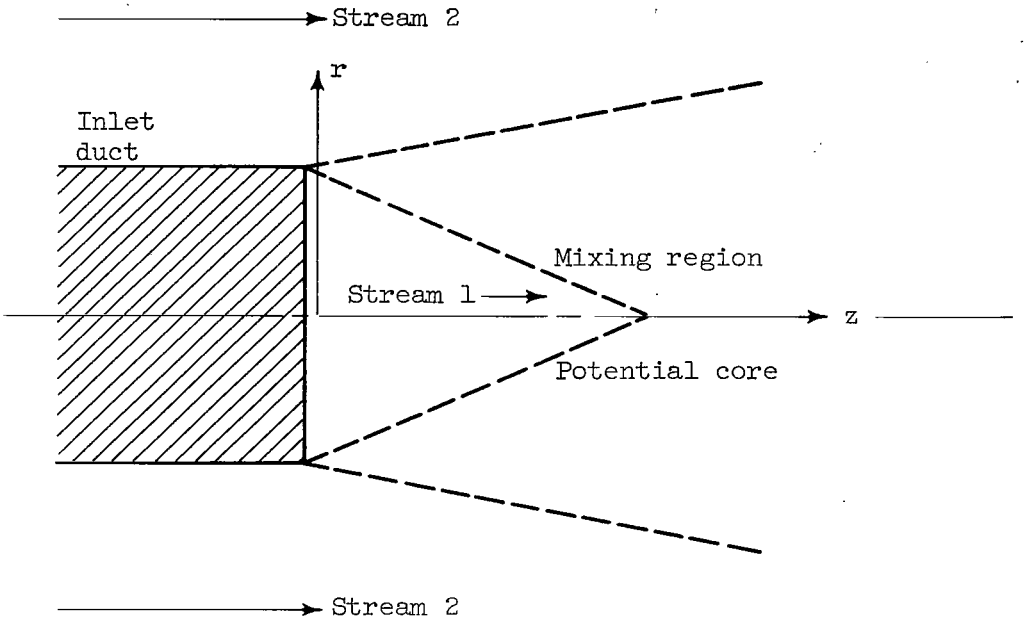

Figure 1. - Flow system.

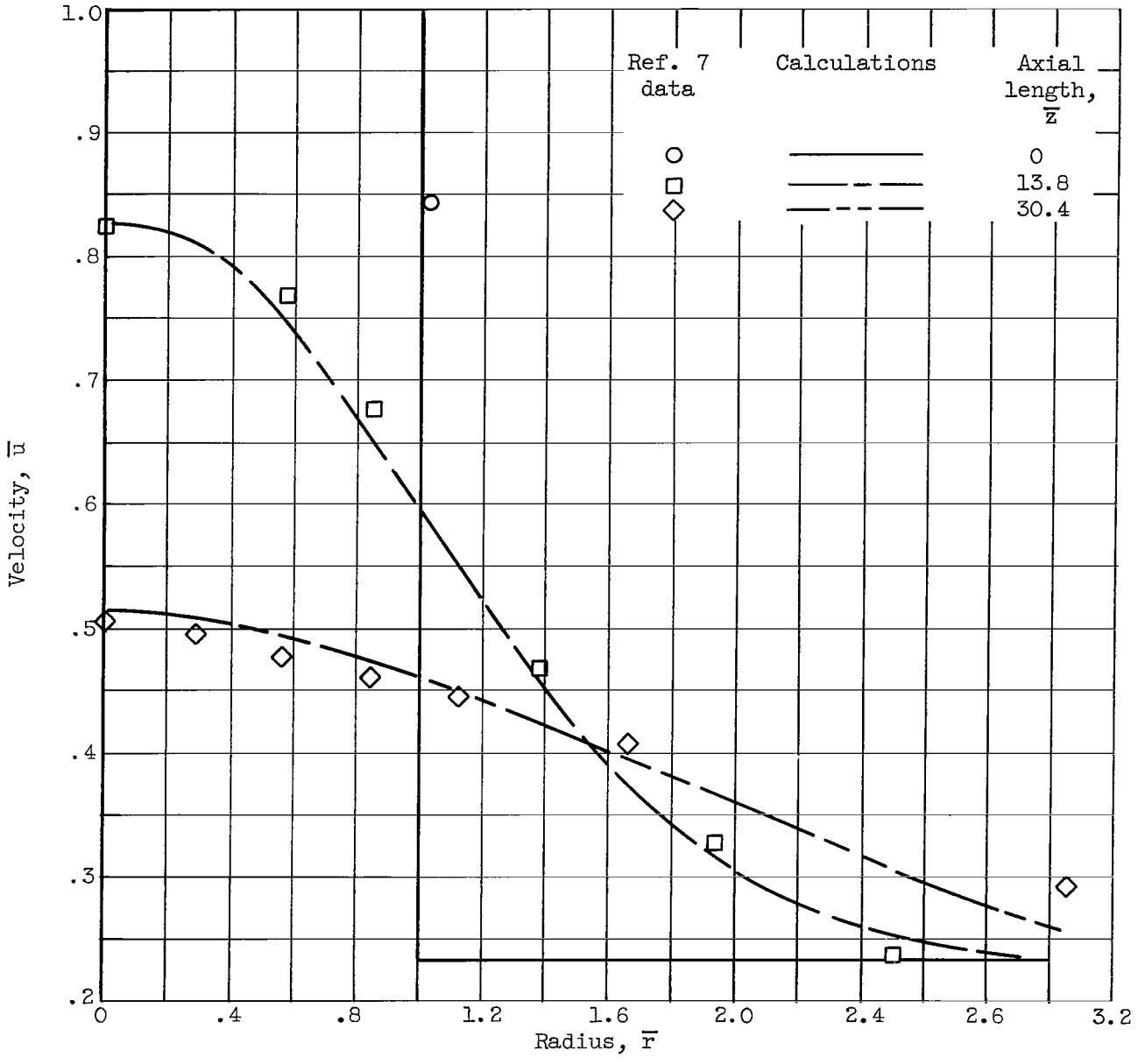

(a) Velocity profiles.

Figure 2. - Analytical fit of data from reference 7.

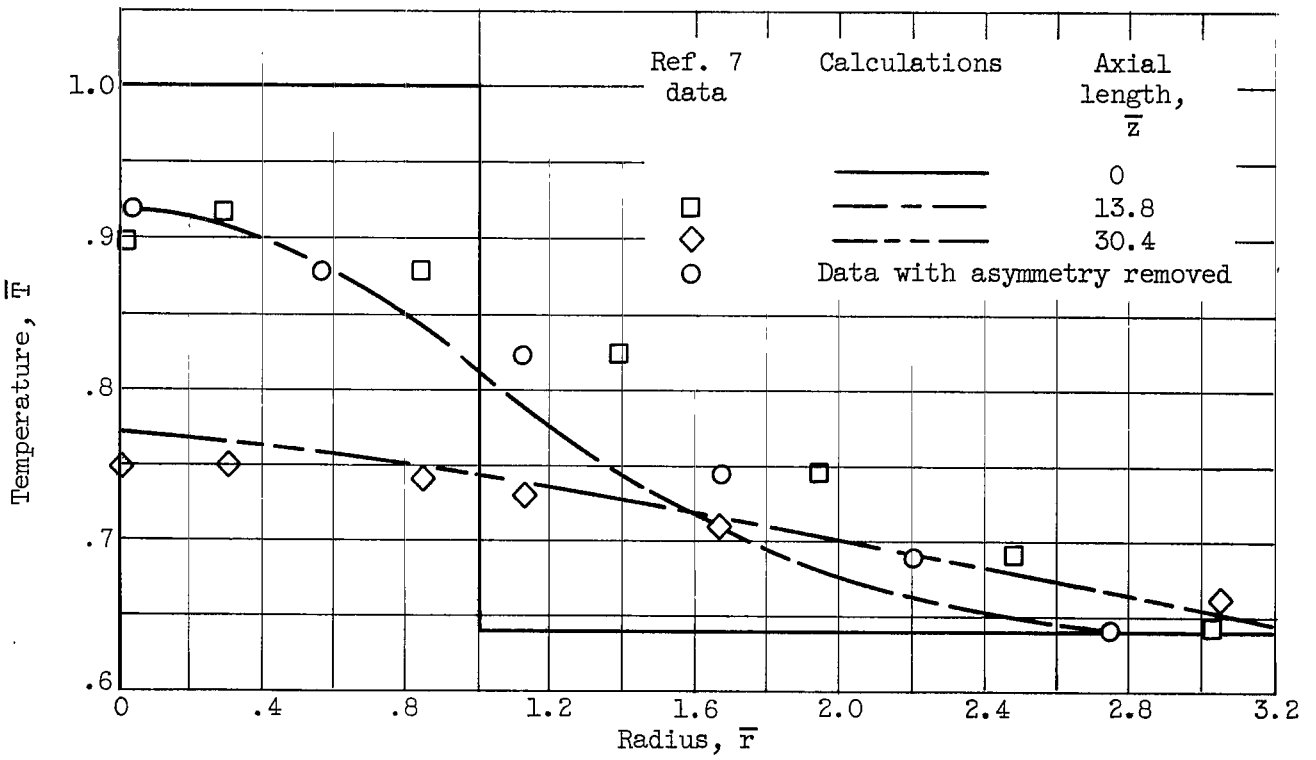

(b) Temperature profiles.

Figure 2. - Concluded. Analytical fit of data from reference 7.

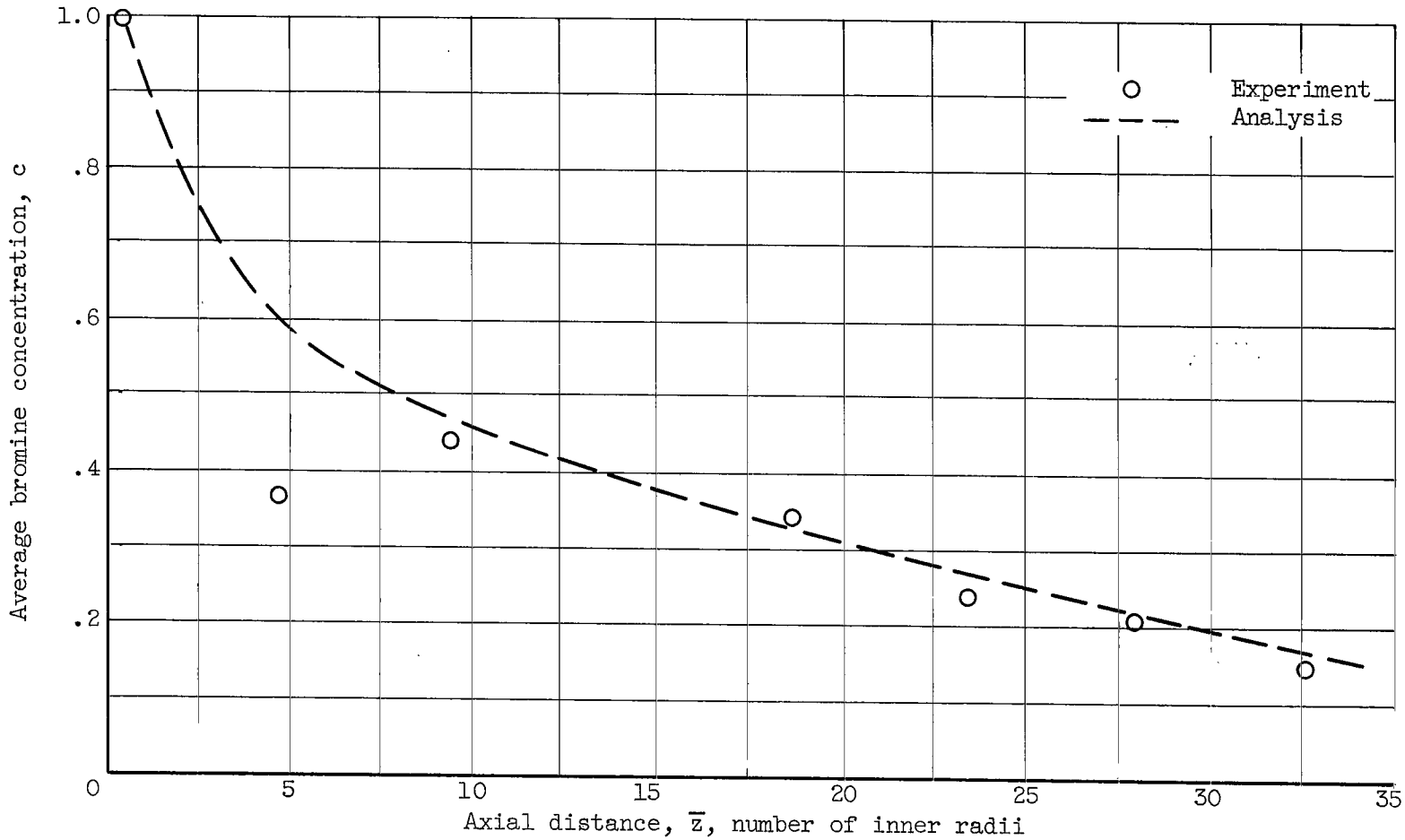

(a) Laminar flow. Air Reynolds number, 1038; bromine Reynolds number, 200; initial ratio of outer- to inner-stream velocity, 4.3.

Figure 3. - Data from air-bromine coaxial-flow tests of reference 4.

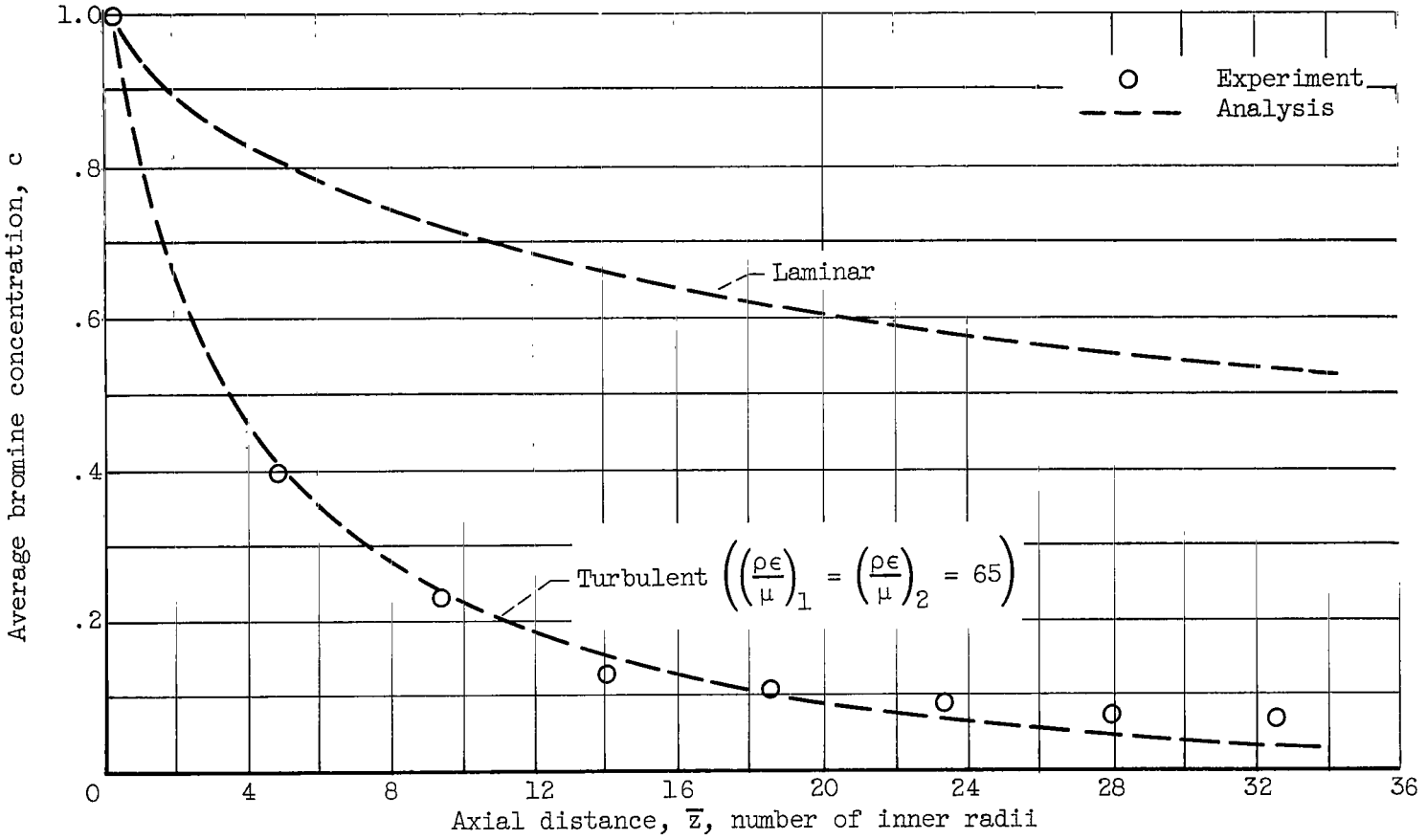

(b) Turbulent flow. Air Reynolds number, 8308; bromine Reynolds number, 1186; initial ratio of outer- to inner-stream velocity, 4.4. (Mass density, ρ; eddy diffusivity, ϵ; viscosity, μ; subscript 1, inner stream; subscript 2, outer stream.)

Figure 3. - Concluded. Data from air-bromine coaxial-flow tests of reference 4.

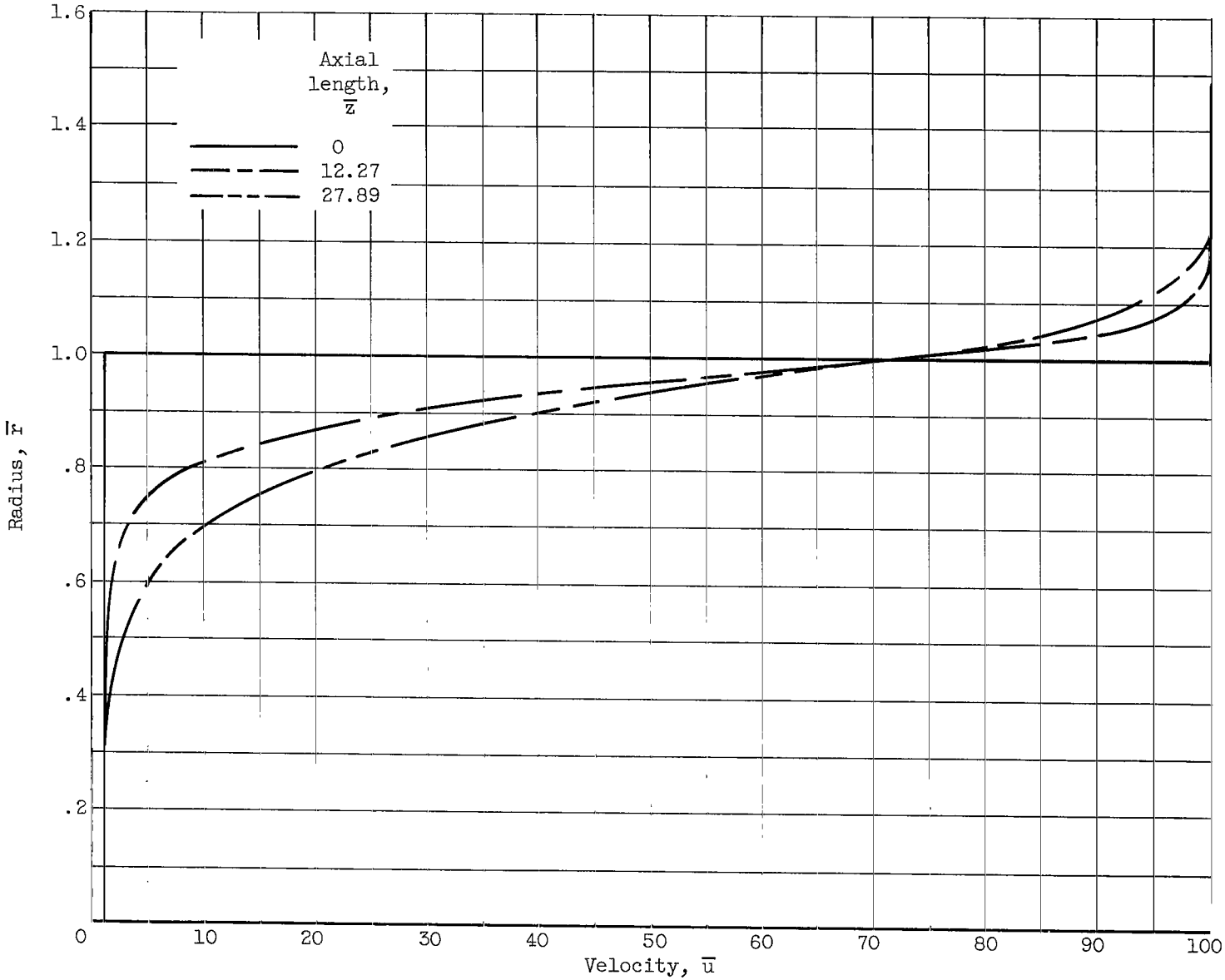

(a) No energy generation.

Figure 4. - Velocity profiles for laminar flow.

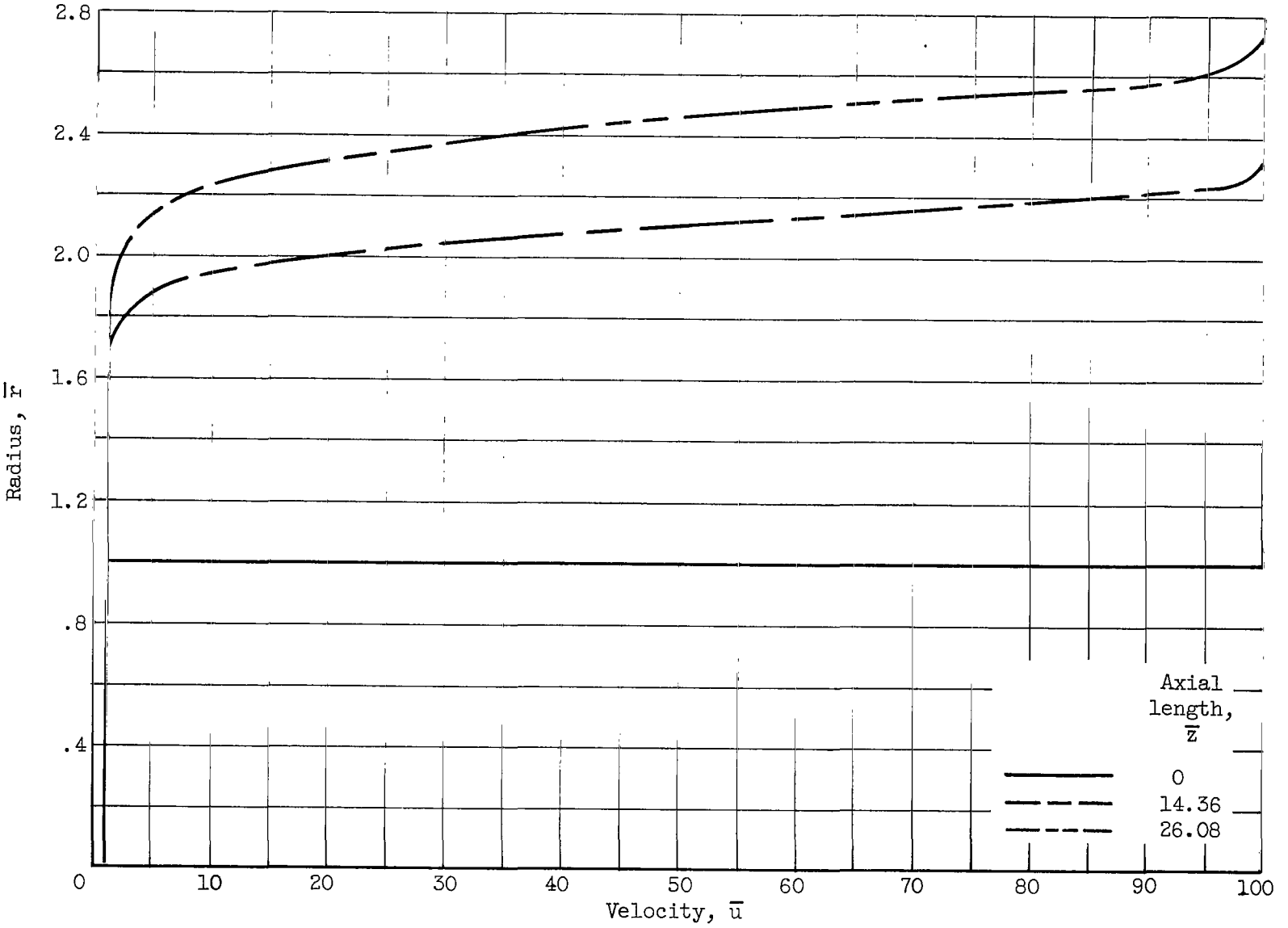

(b) Energy generation; no wall assumption; energy-generation term $G = c/T$, where c is inner-stream concentration and T is temperature.

Figure 4. - Continued. Velocity profiles for laminar flow.

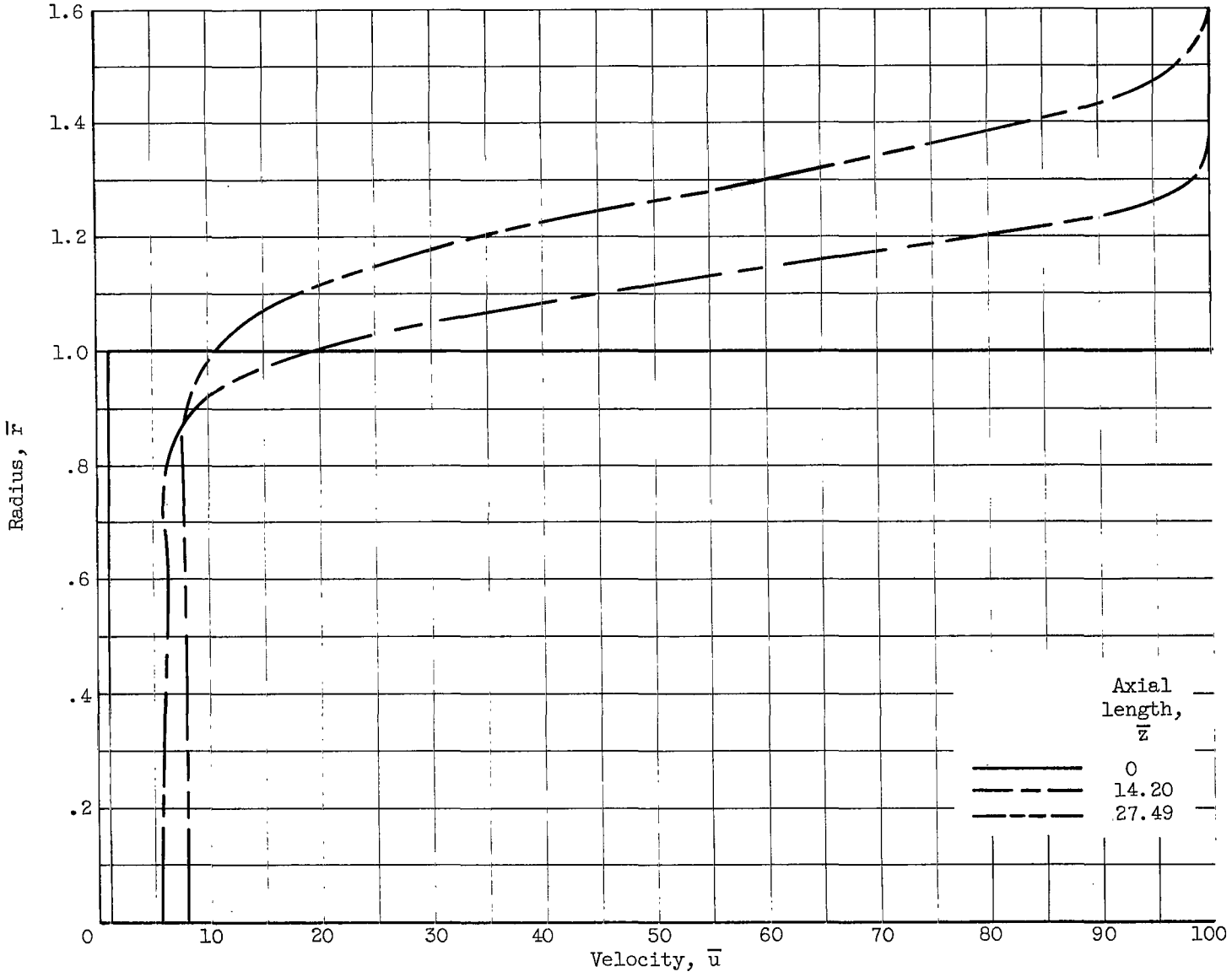

(c) Energy generation; wall assumption; energy-generation term $G = c/T$, where c is inner-stream concentration and T is temperature.

Figure 4. - Concluded. Velocity profiles for laminar flow.

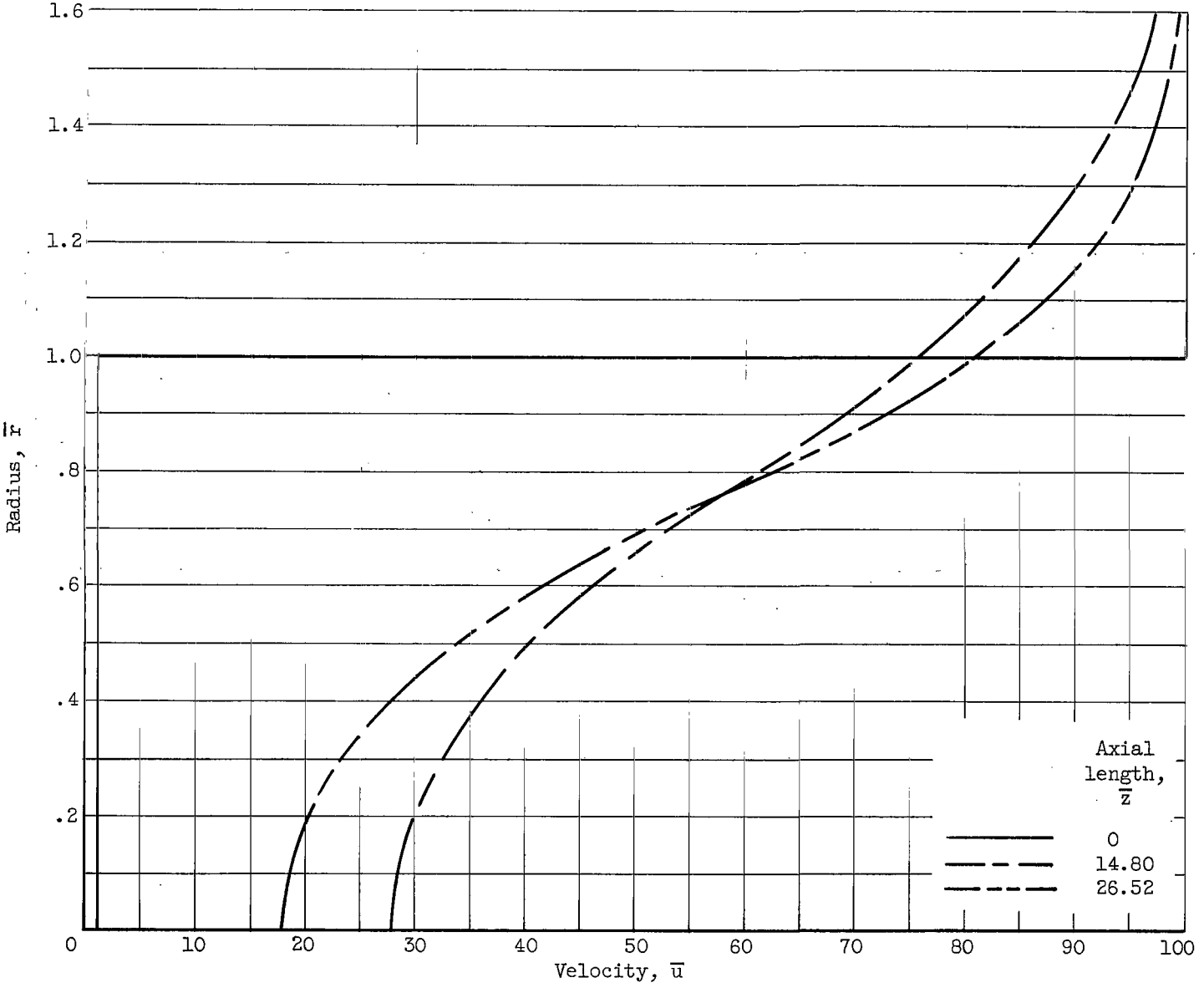

(a) No energy generation.

Figure 5. - Velocity profiles for turbulent flow. Flow factor, 23.

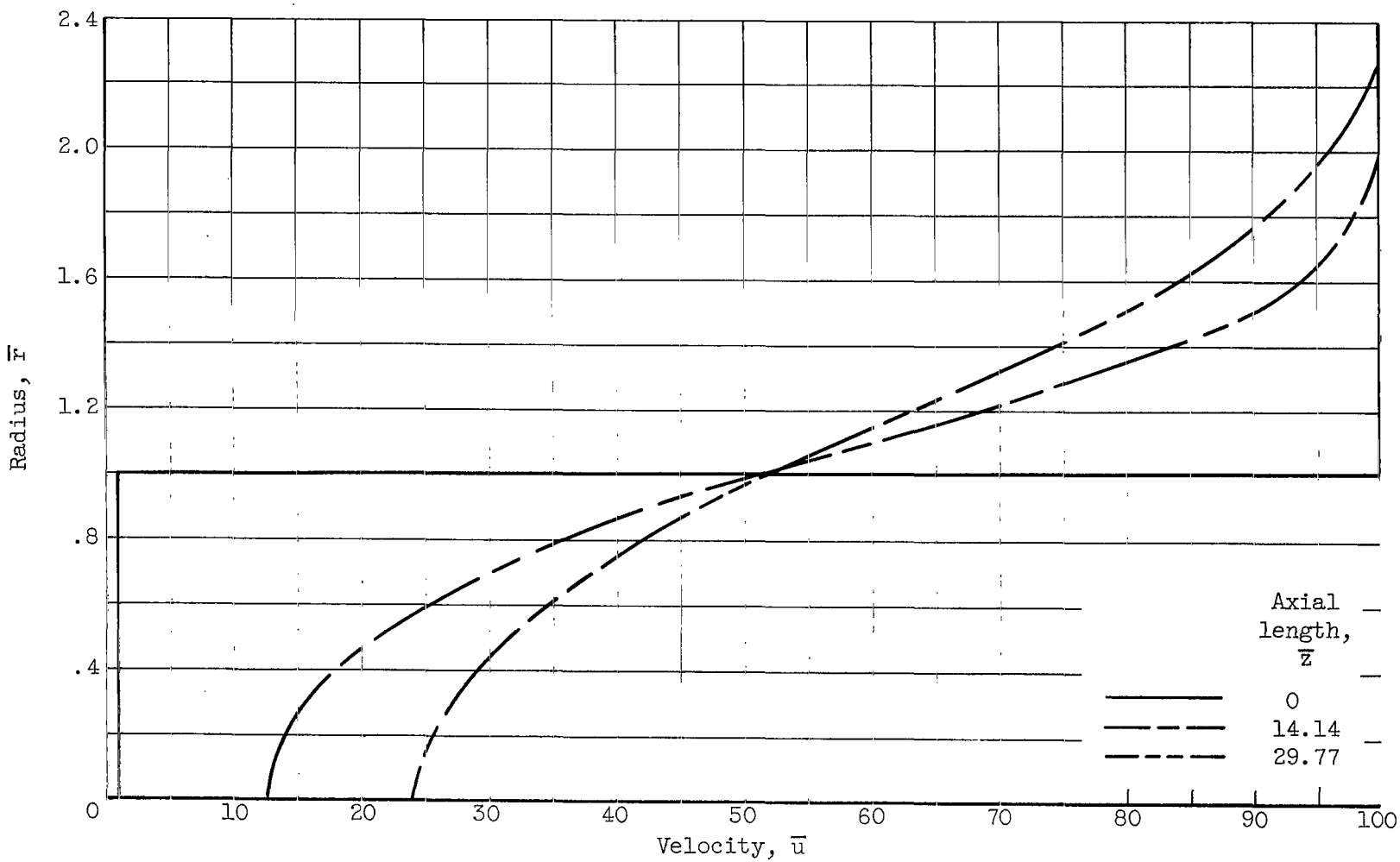

(b) Energy generation; no wall assumption; energy-generation term $G = c/T$, where c is inner-stream concentration and T is temperature.

Figure 5. - Continued. Velocity profiles for turbulent flow. Flow factor, 23.

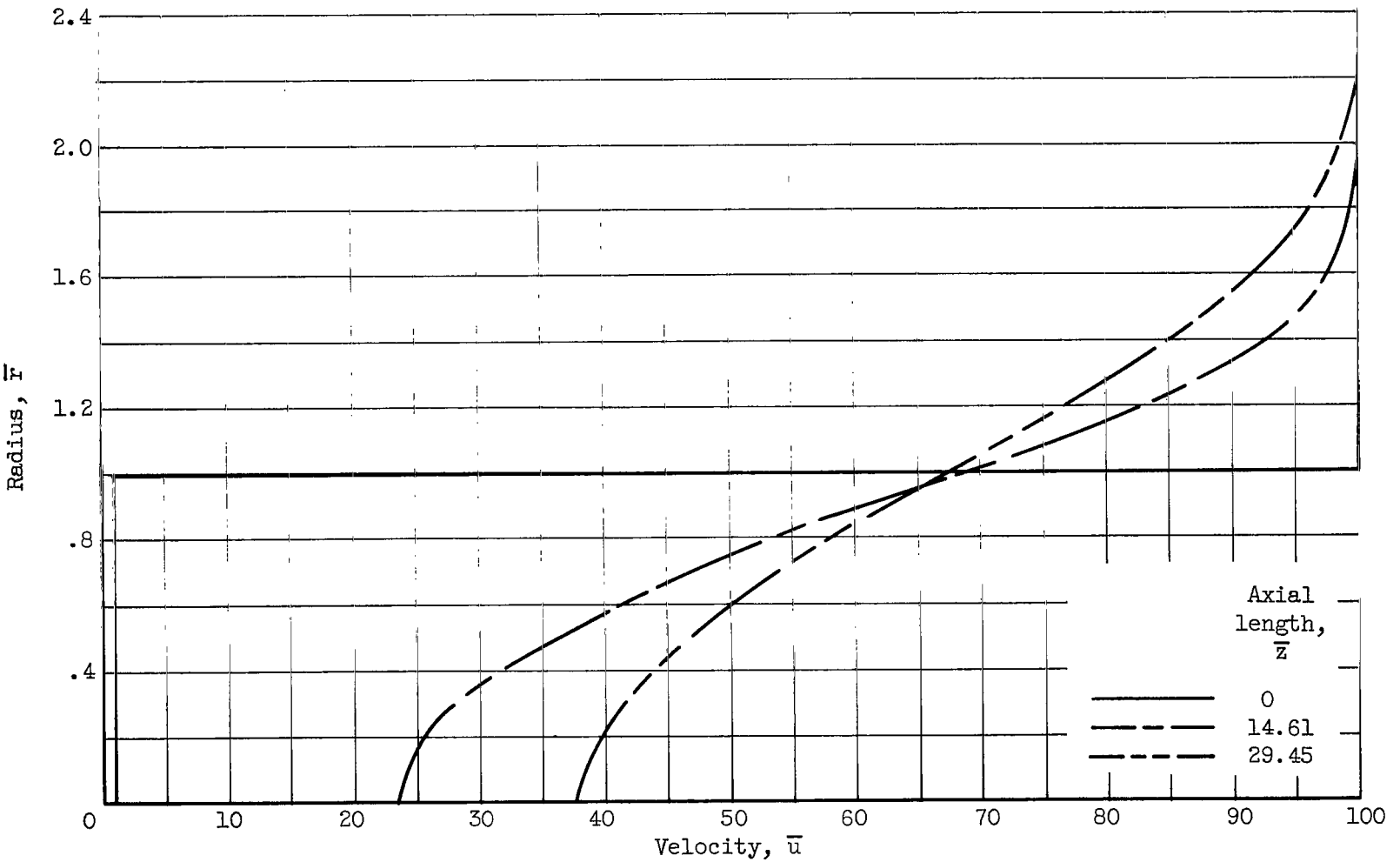

(c) Energy generation; wall assumption; energy-generation term $G = c/T$, where c is inner-stream concentration and T is temperature.

Figure 5. - Concluded. Velocity profiles for turbulent flow. Flow factor, 23.

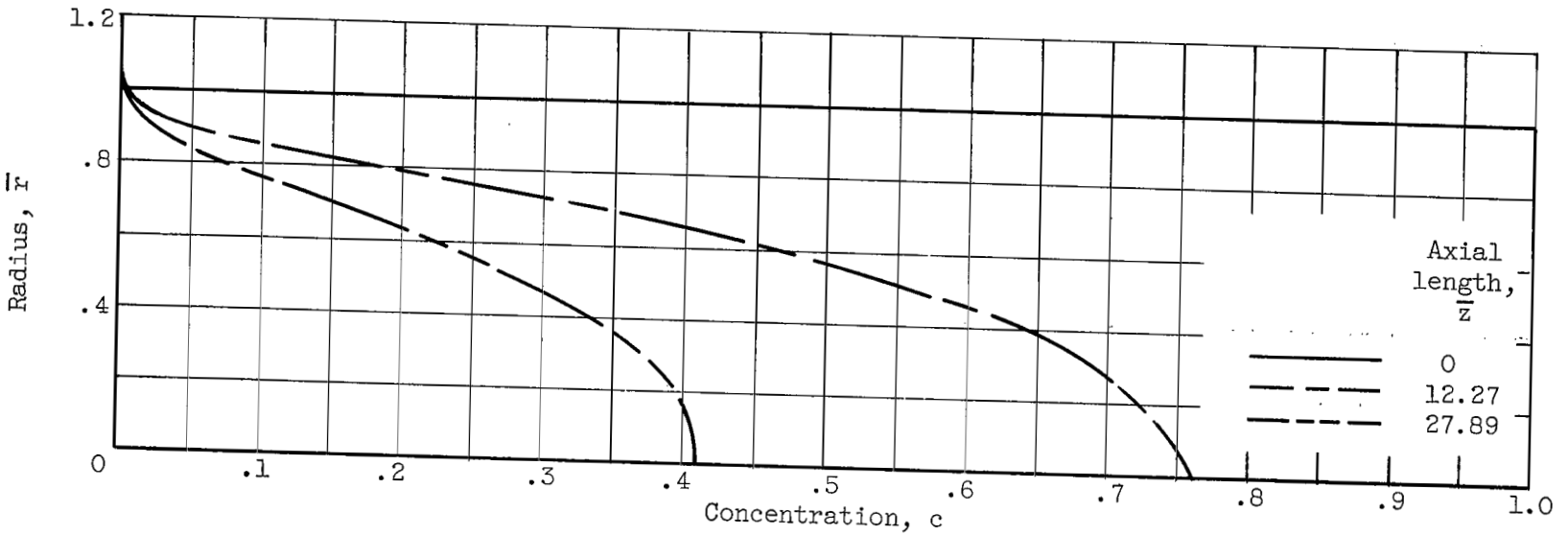

(a) No energy generation.

Figure 6. - Concentration profiles for laminar flow.

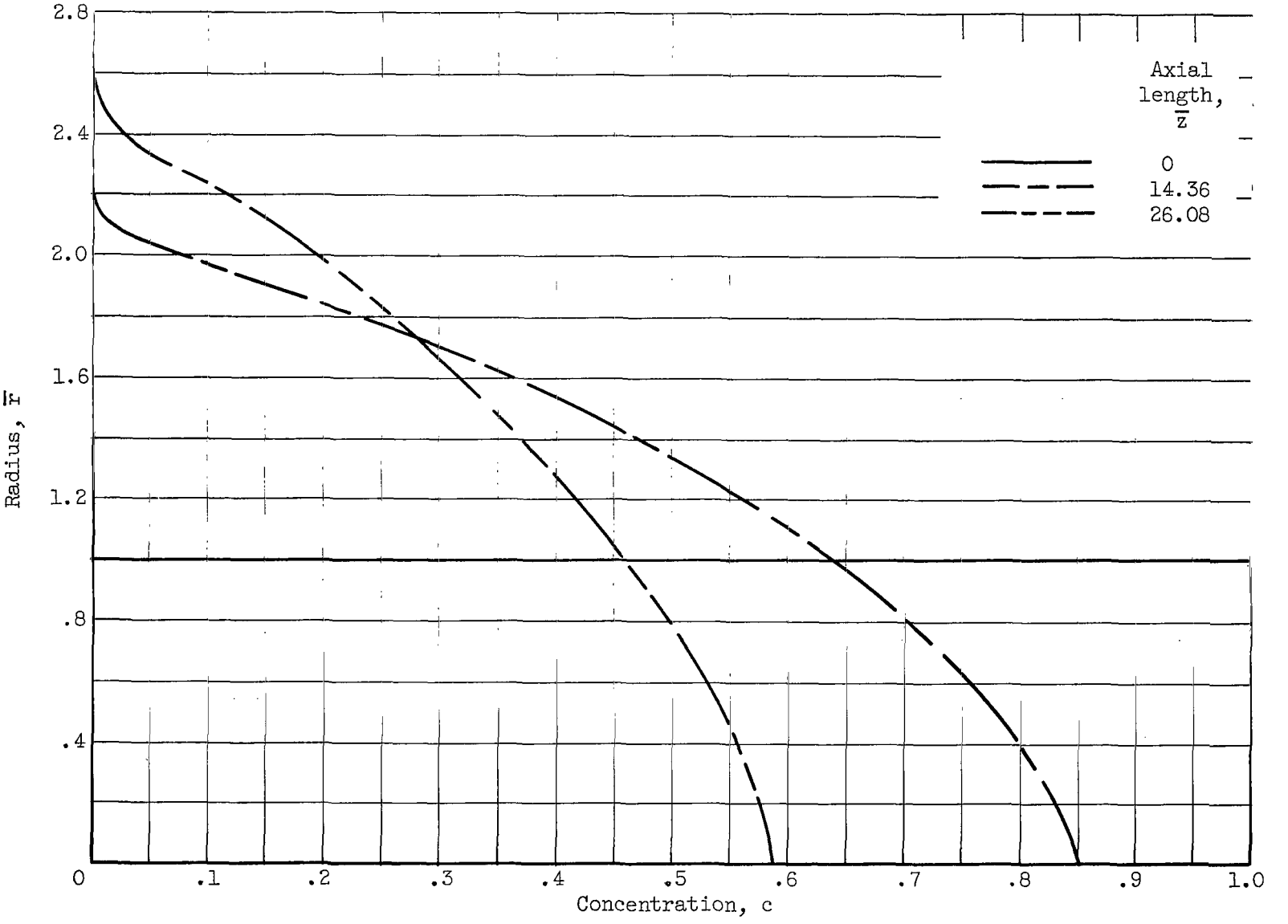

(b) Energy generation; no wall assumption; energy-generation term $G = c/T$, where c is inner-stream concentration and T is temperature.

Figure 6. - Continued. Concentration profiles for laminar flow.

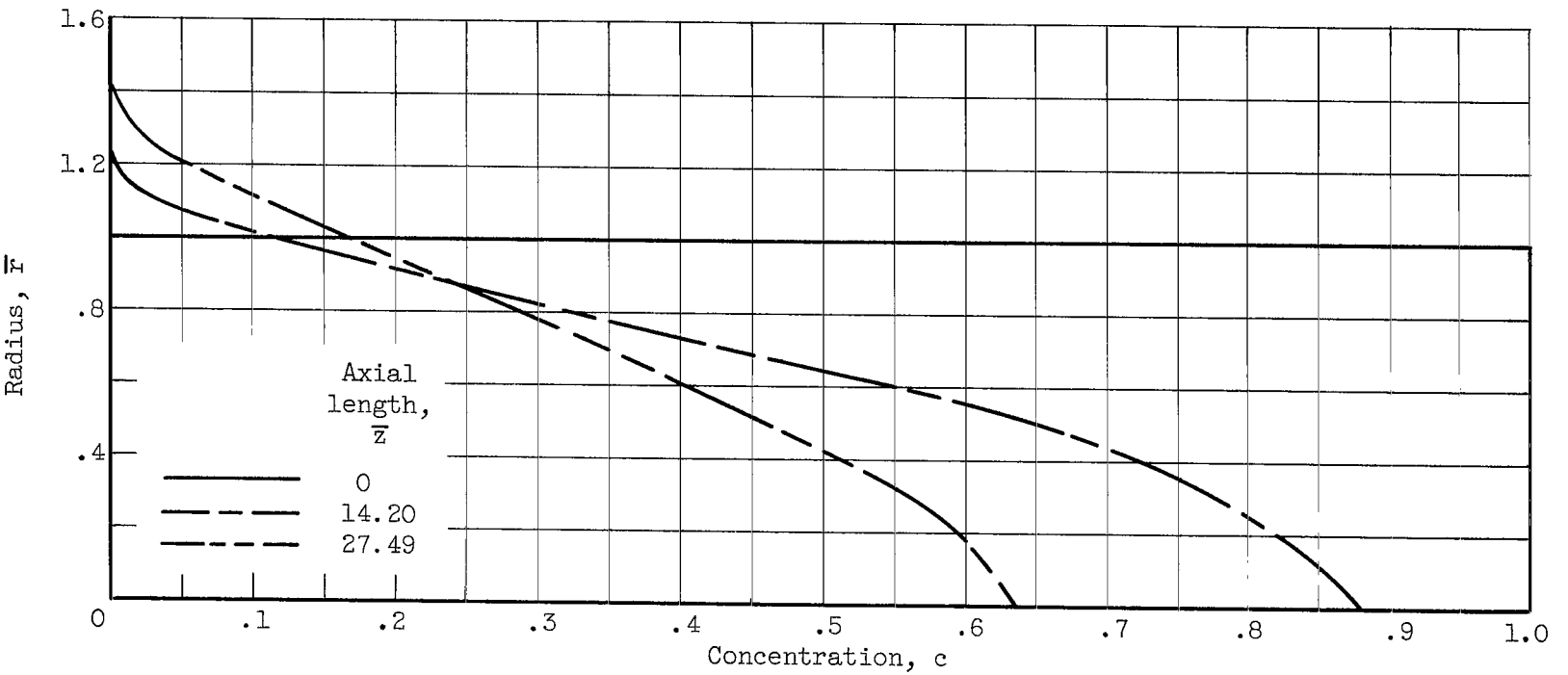

(c) Energy generation; wall assumption; energy-generation term $G = c/T$, where c is inner-stream concentration and T is temperature.

Figure 6. - Concluded. Concentration profiles for laminar flow.

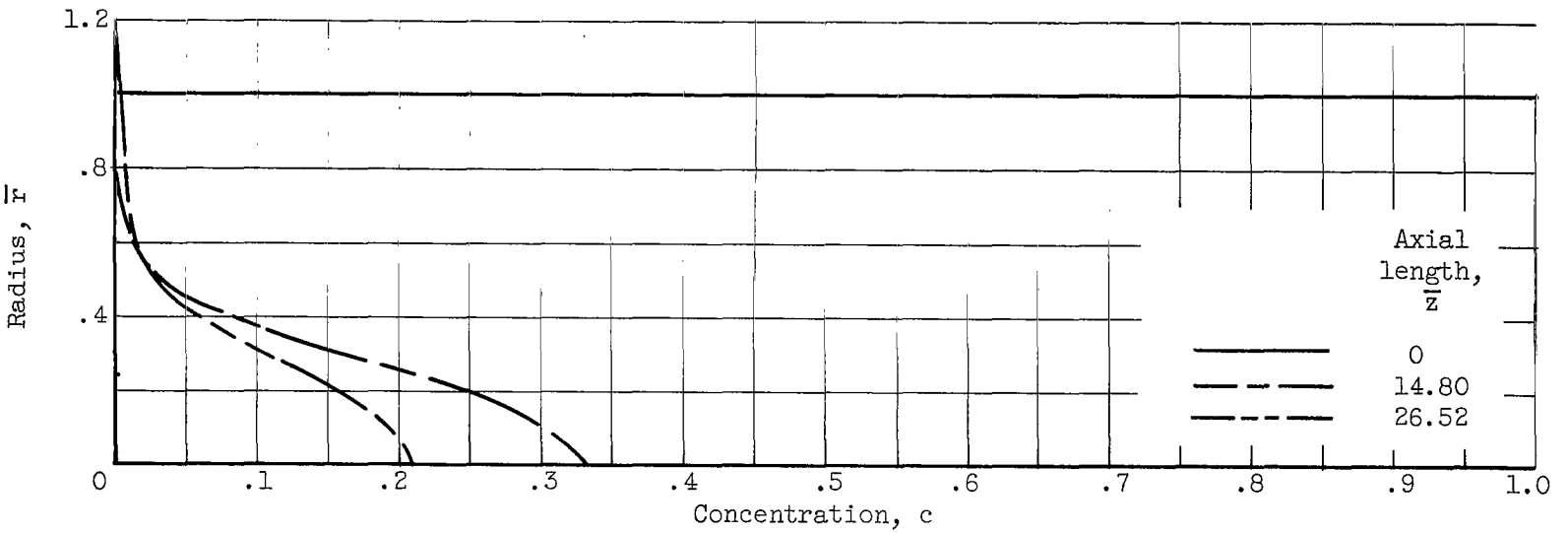

(a) No energy generation.

Figure 7. - Concentration profiles for turbulent flow. Flow factor, 23.

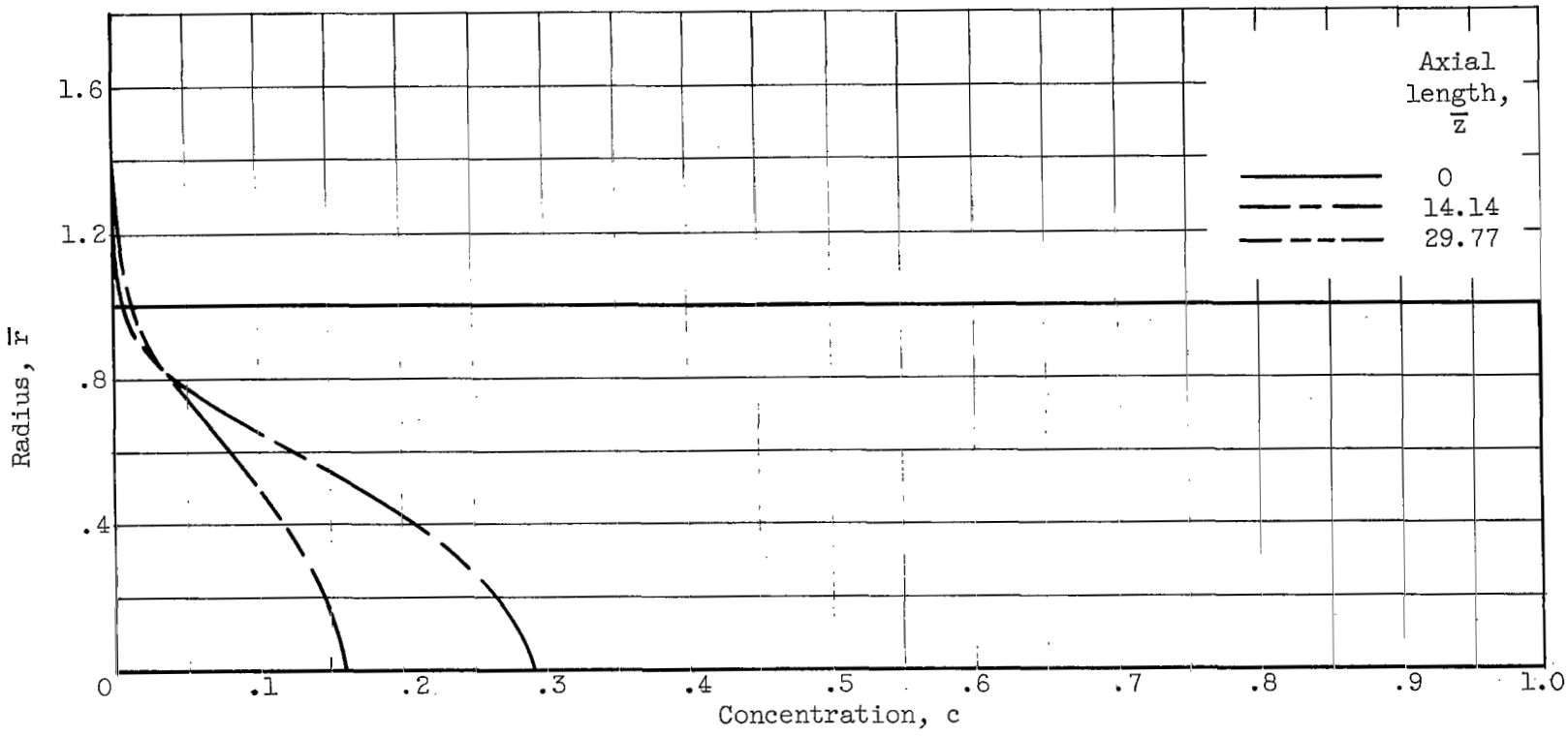

(b) Energy generation; no wall assumption; energy-generation term $G = c/T$, where c is inner-stream concentration and T is temperature.

Figure 7. - Continued. Concentration profiles for turbulent flow. Flow factor, 23.

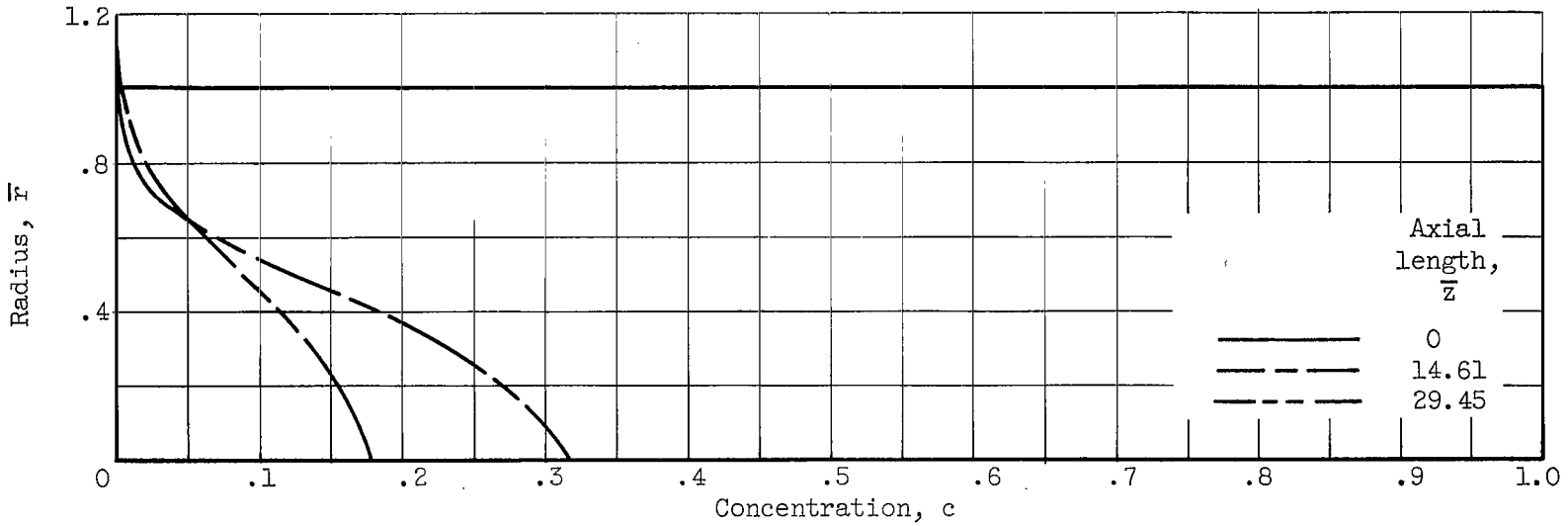

(c) Energy generation; wall assumption; energy-generation term $G = c/T$, where c is inner-stream concentration and T is temperature.

Figure 7. - Concluded. Concentration profiles for turbulent flow. Flow factor, 23.

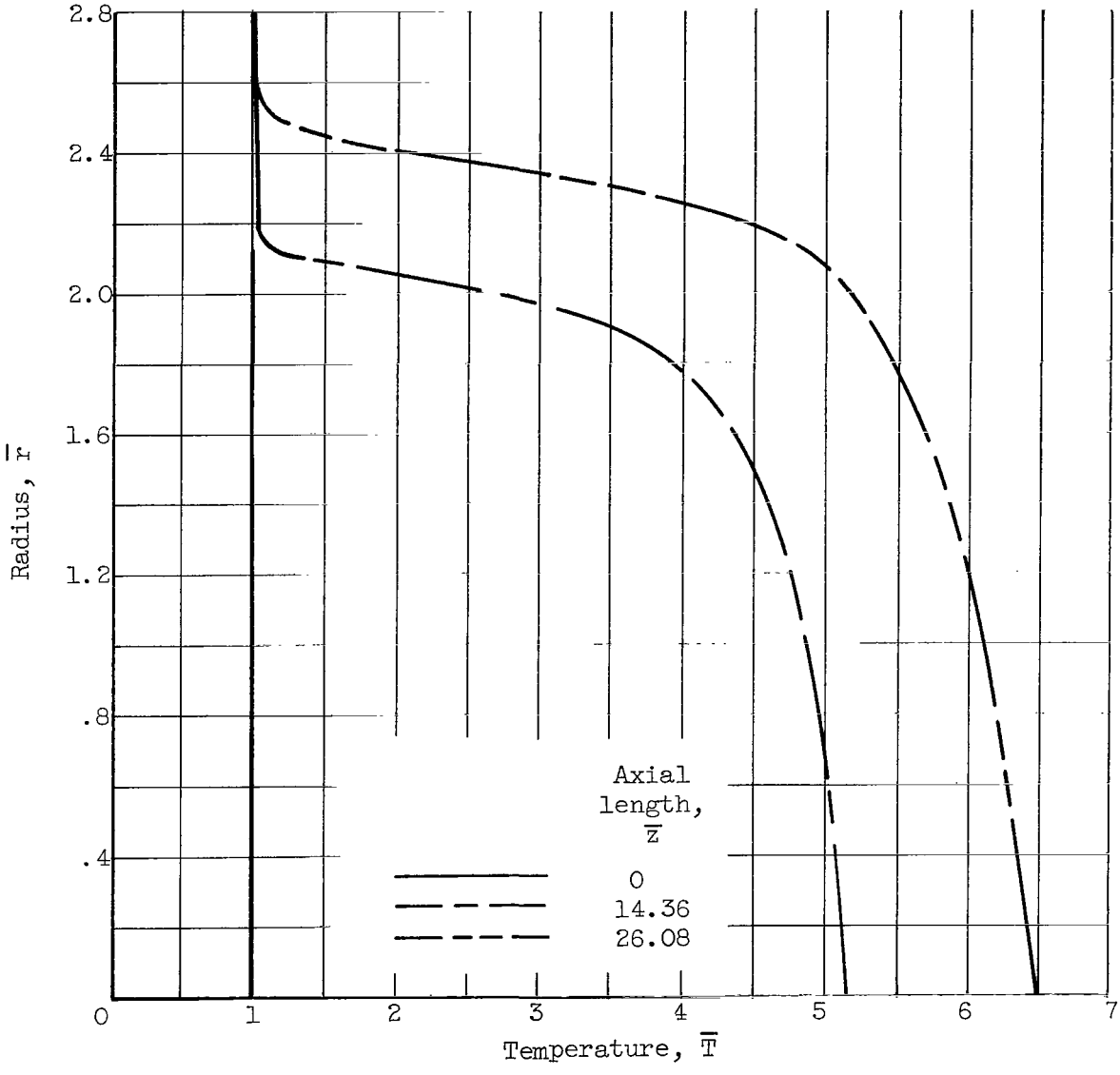

(a) No wall assumption.

Figure 8. - Temperature profiles for laminar flow with energy generation. Energy-generation term $G = c/T$, where c is inner-stream concentration and T is temperature.

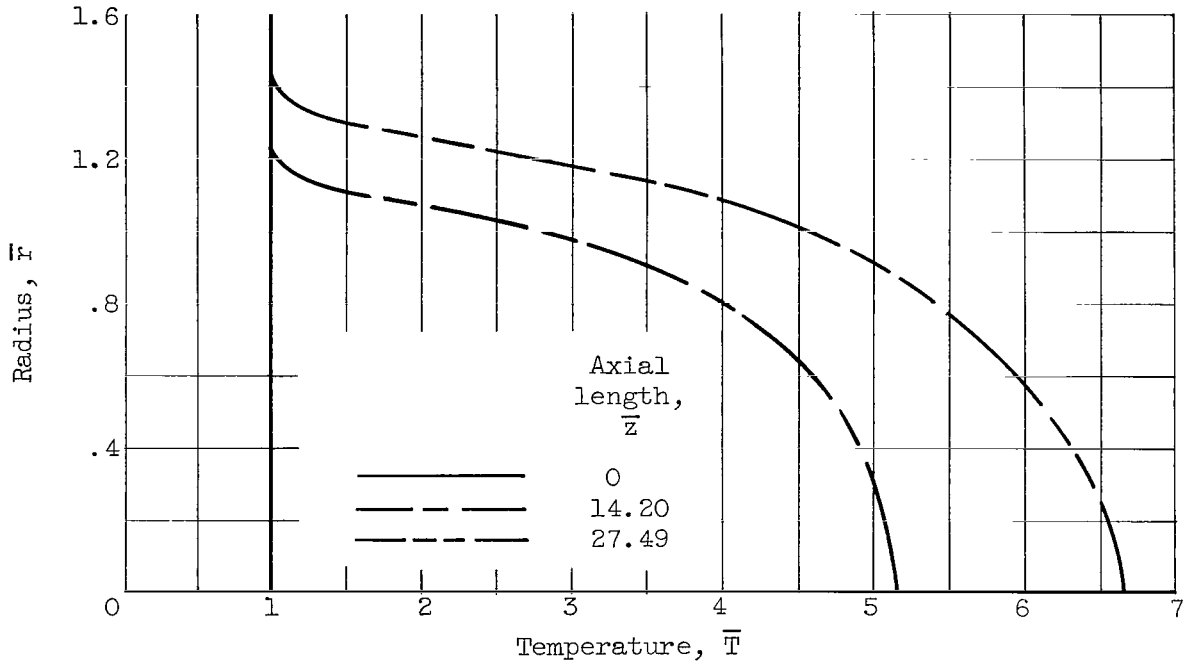

(b) Wall assumption.

Figure 8. - Concluded. Temperature profiles for laminar flow with energy generation. Energy-generation term $G = c/T$, where c is inner-stream concentration and T is temperature.

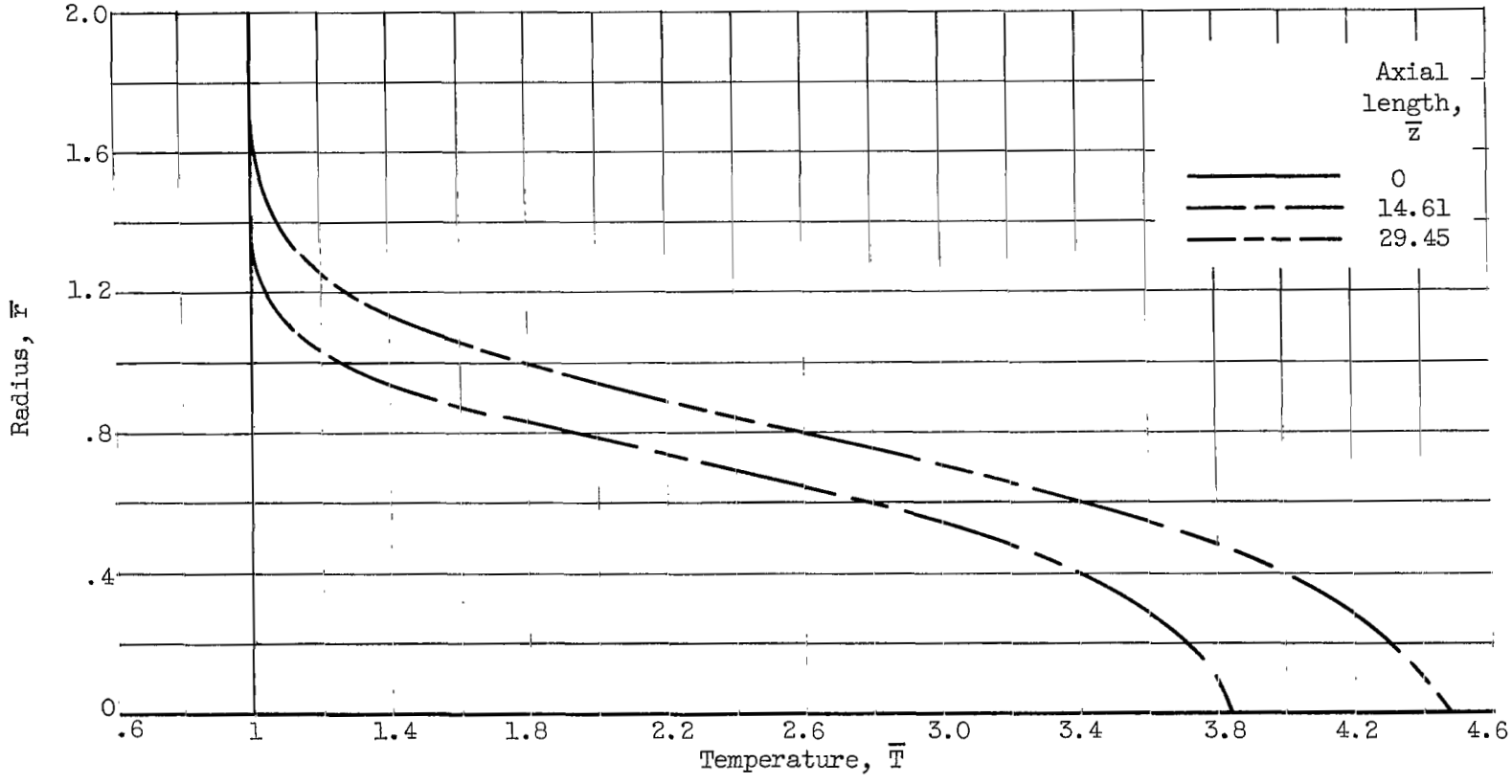

(a) No wall assumption.

Figure 9. - Temperature profiles for turbulent flow with energy generation. Flow factor, 23; energy-generation term $G = c/T$, where c is inner-stream concentration and T is temperature.

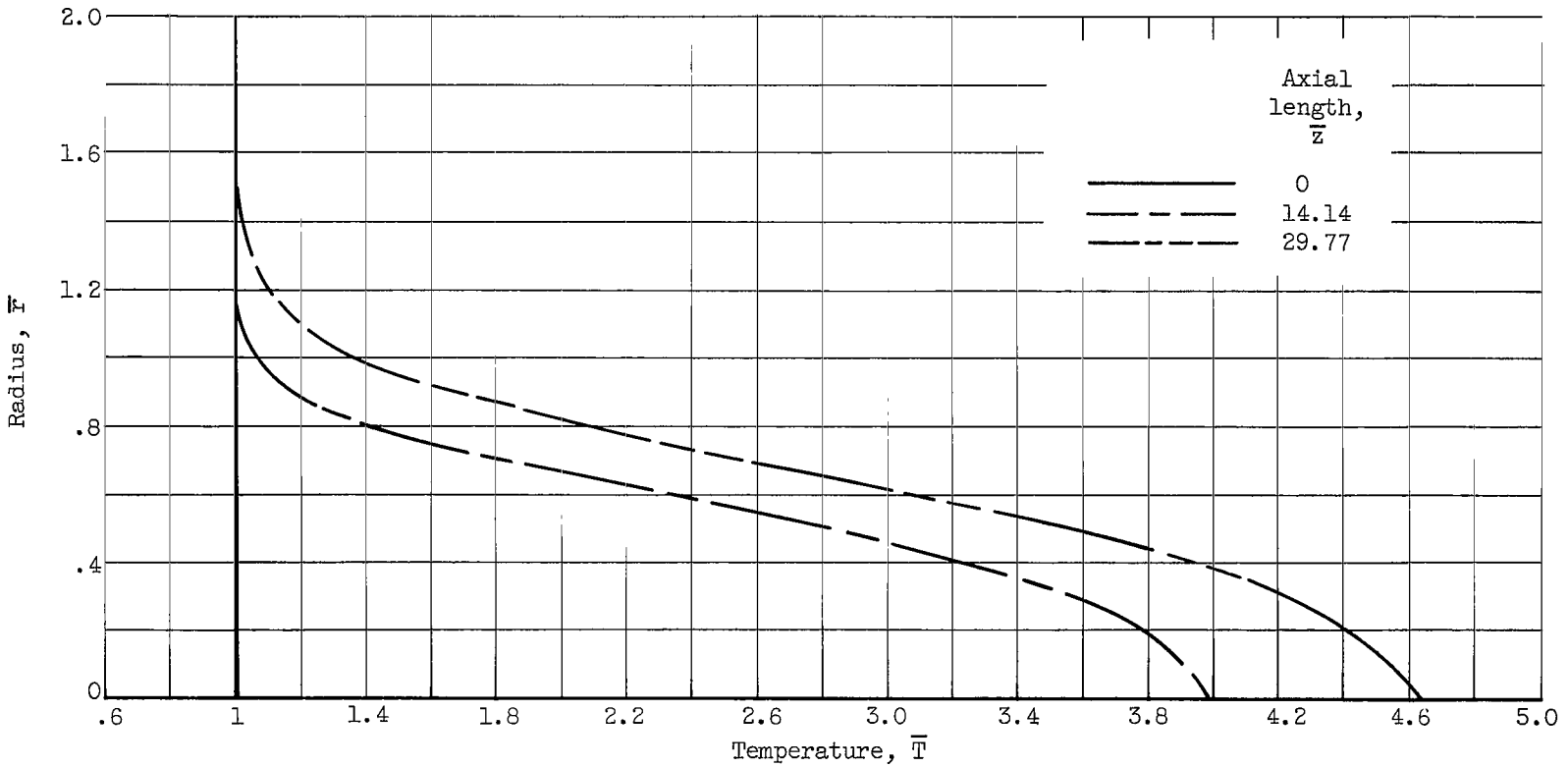

(b) Wall assumption.

Figure 9. - Concluded. Temperature profiles for turbulent flow with energy generation. Flow factor, 23; energy-generation term $G = c/T$, where c is inner-stream concentration and T is temperature.

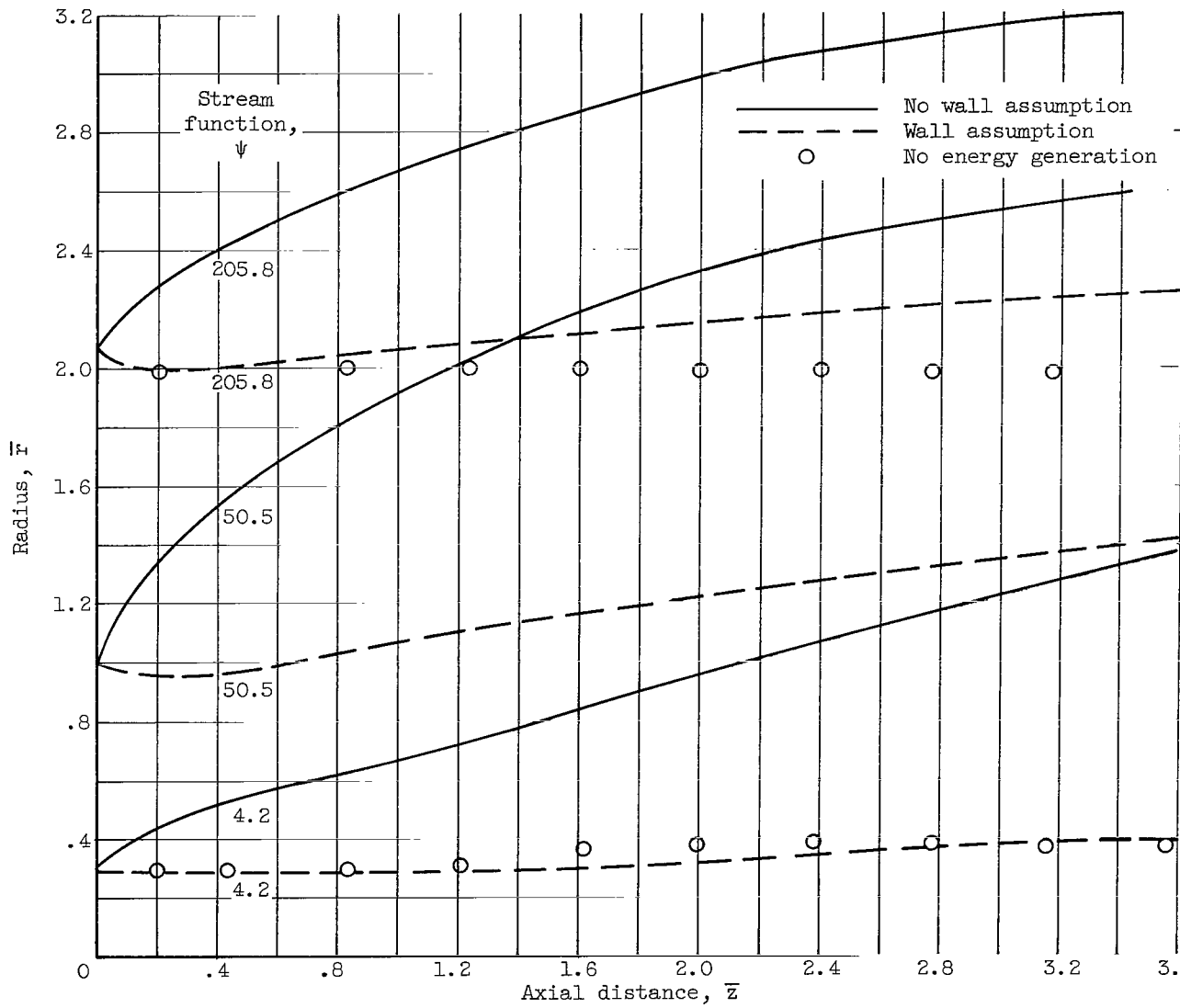

(a) Laminar flow.

Figure 10. - Effect of energy-generation assumption on streamlines. Energy-generation term $G = c/T$, where c is inner-stream concentration and T is temperature.

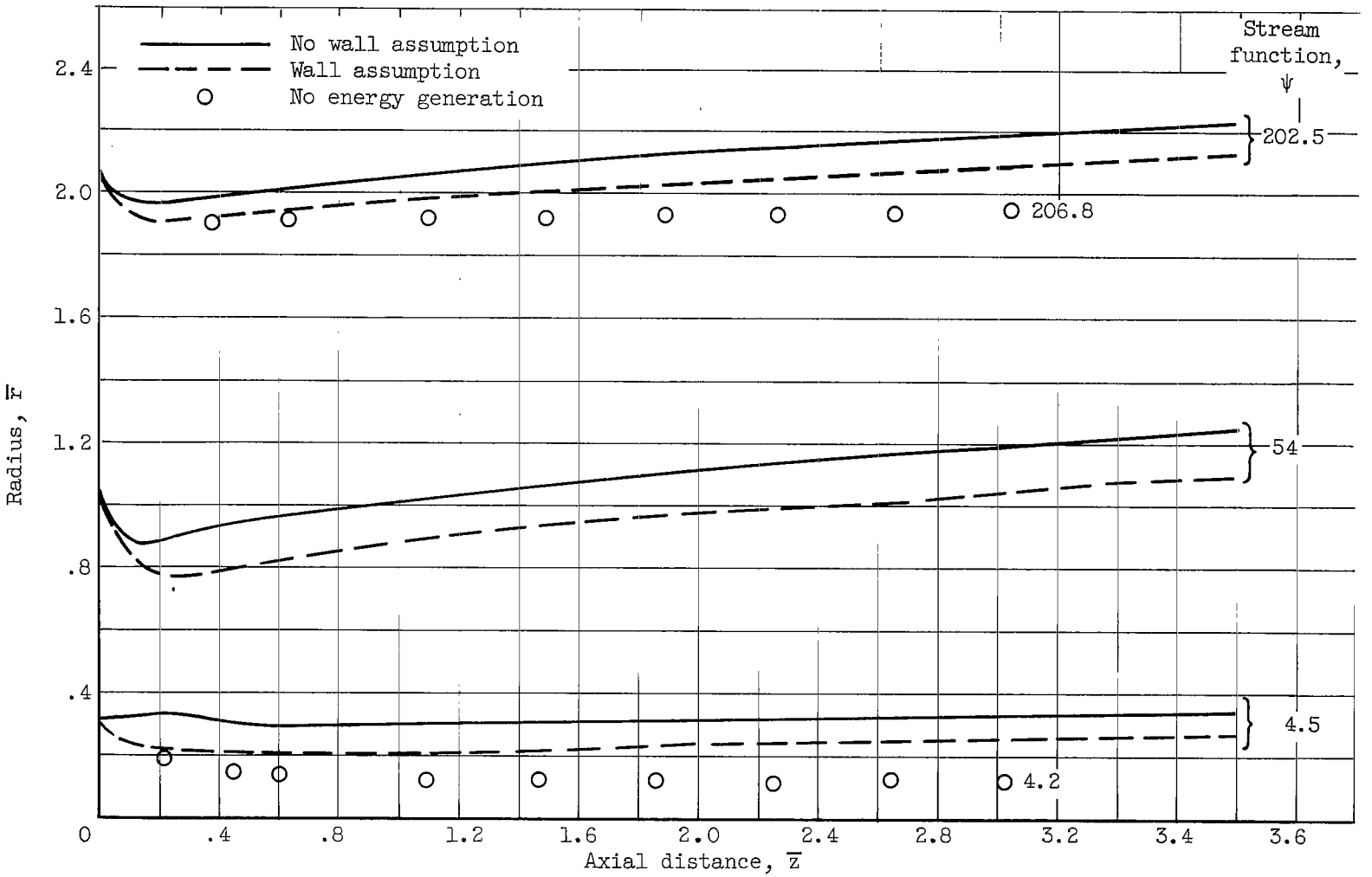

(b) Turbulent flow. Flow factor, 23.

Figure 10. - Concluded. Effect of energy-generation assumption on streamlines. Energy-generation term $G = c/T$, where c is inner-stream concentration and T is temperature.

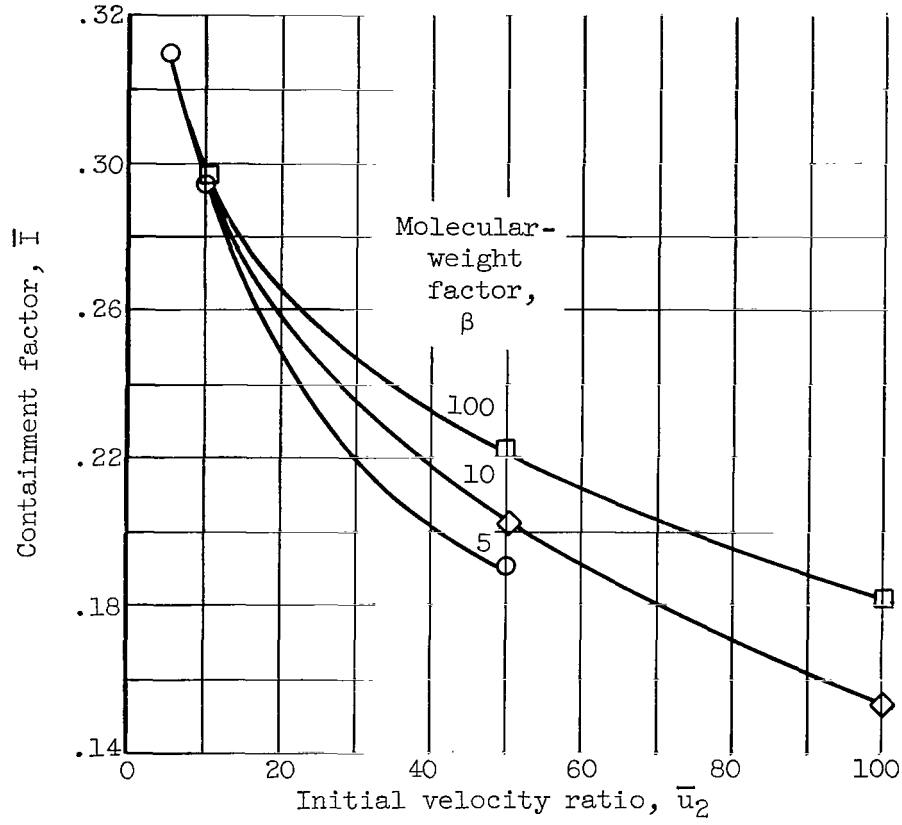

(a) Laminar flow with energy generation in inner stream. Energy-generation term $G = 0.3c/T$, where c is inner-stream concentration and T is temperature.

Figure 11. - Effect of variation of initial velocity ratio on containment factor. Reynolds number, 1000; Schmidt number, 1; Prandtl number, 1; molecular volume, 0.47; initial velocity ratio, 0.20; initial specific heat, $\beta + 1$; initial conductivity ratio, 25; length, 30; wall assumption.

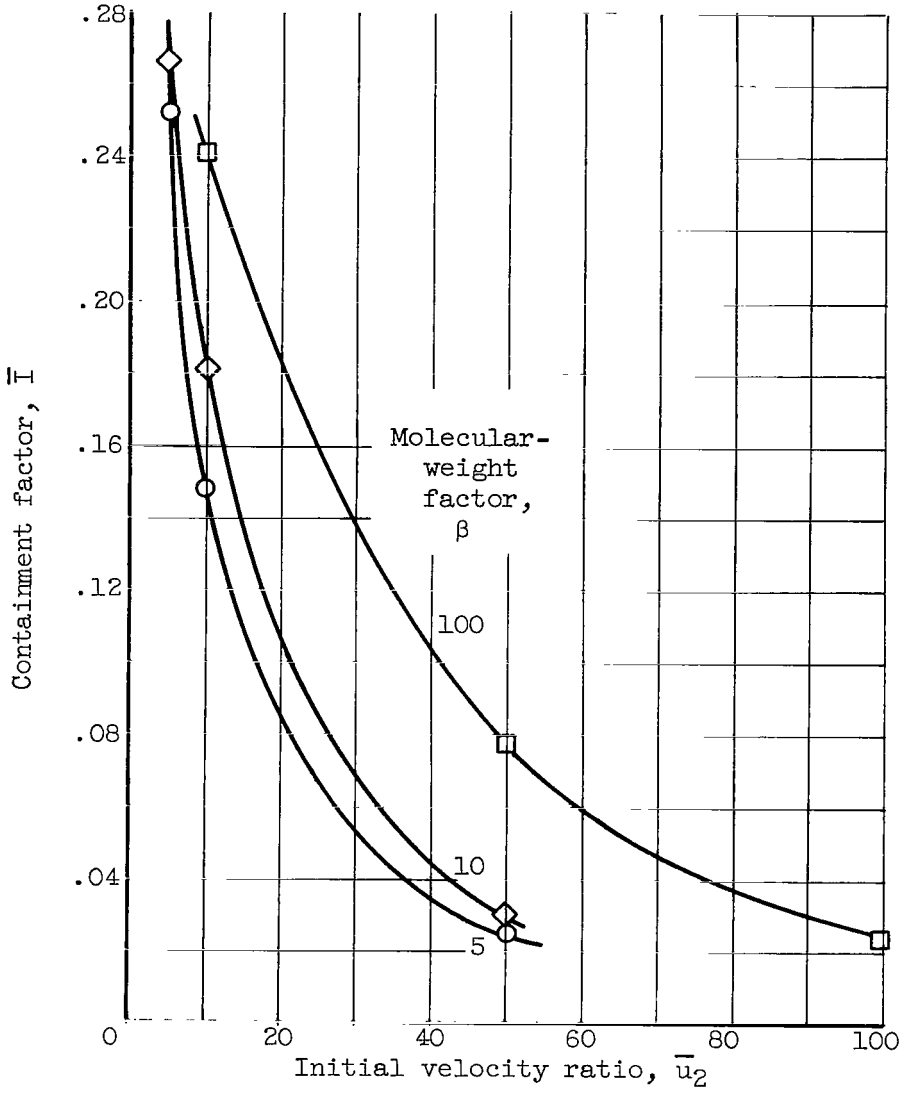

(b) Turbulent flow with energy generation in inner stream. Energy generation term $G = 0.5c/T$, where c is inner-stream concentration and T is temperature.

Figure 11. - Continued. Effect of variation of initial velocity ratio on containment factor. Reynolds number, 1000; Schmidt number, 1; Prandtl number, 1; molecular volume, 0.47; initial velocity ratio, 0.20; initial specific heat, $\beta + 1$; initial conductivity ratio, 25; length, 30; wall assumption.

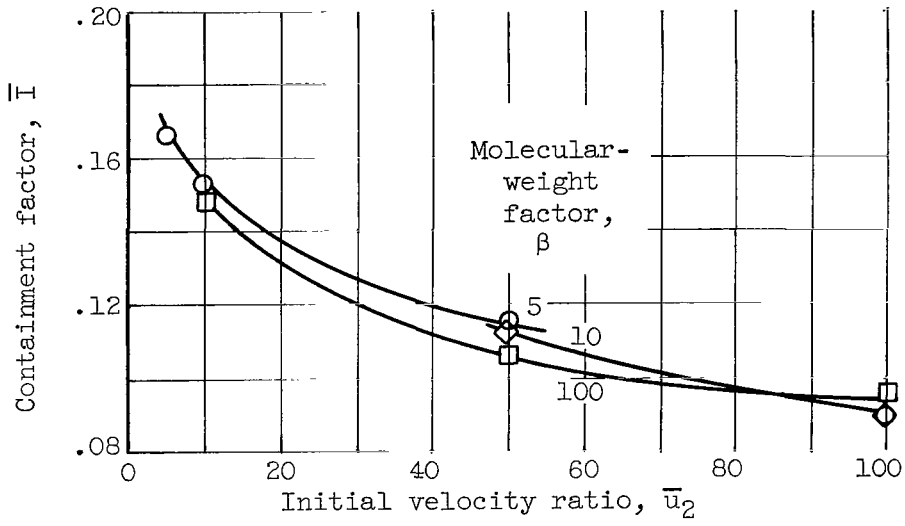

(c) Laminar flow with energy generation in both streams. Energy generation term $G = 0.3c/T + 0.3$, where c is inner-stream concentration and T is temperature.

Figure 11. - Continued. Effect of variation of initial velocity ratio on containment factor. Reynolds number, 1000; Schmidt number, 1; Prandtl number, 1; molecular volume, 0.47; initial velocity ratio, 0.20; initial specific heat, $\beta + 1$; initial conductivity ratio, 25; length, 30; wall assumption.

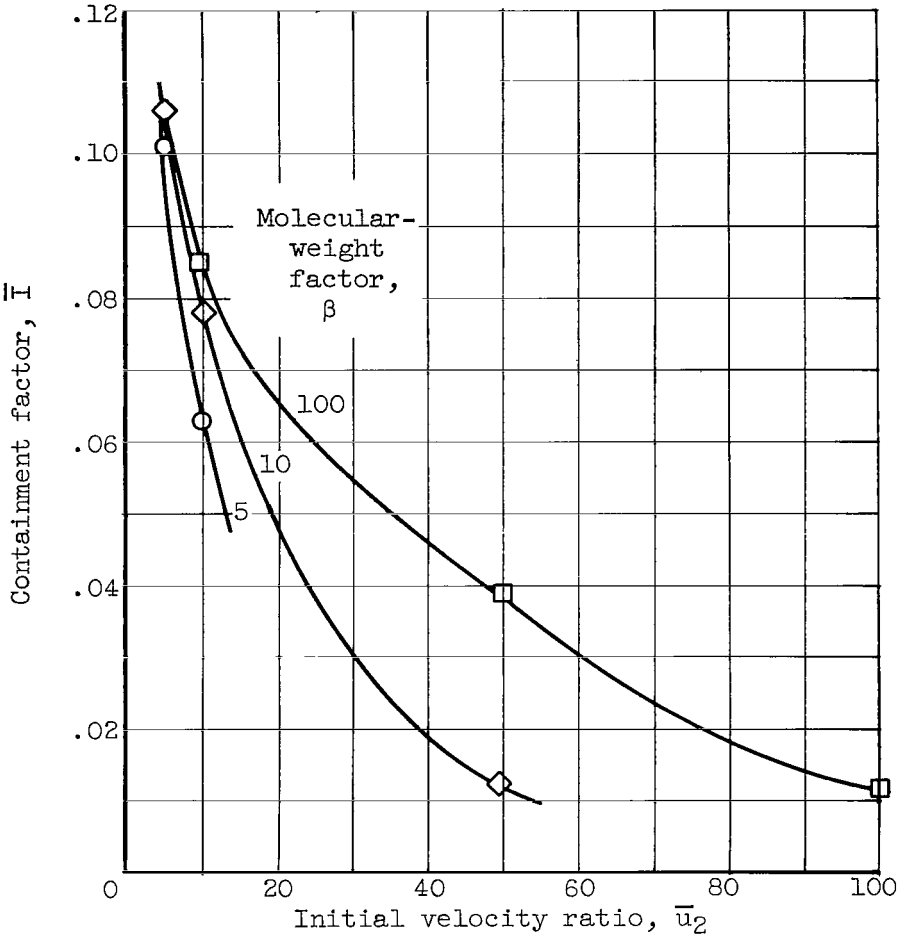

(d) Turbulent flow with energy generation in both streams. Energy generation term, $G = 0.5c/T + 0.5$, where c is inner-stream concentration and T is temperature.

Figure 11. - Concluded. Effect of variation of initial velocity ratio on containment factor. Reynolds number, 1000; Schmidt number, 1; Prandtl number, 1; molecular volume, 0.47; initial velocity ratio, 0.20; initial specific heat, $\beta + 1$; initial conductivity ratio, 25; length, 30; wall assumption.